Ultrafast Vibrational Dynamics of Hydrogen Bonds in the Condensed Phase

Erik T. J. Nibbering and Thomas Elsaesser*

Max-Born-Institut für Nichtlineare Optik und Kurzzeitspektroskopie, Max-Born-Strasse 2 A, D-12489 Berlin, Germany

Received May 20, 2003

Contents

1. Introduction

Hydrogen bonding represents one of the fundamental types of chemical bonding and underlies the structure of a large variety of molecular systems, among them liquids, biological macromolecules, and crystalline structures. Hydrogen bonds are characterized by a binding energy between 1 and 50 kJ/mol, depending on the local geometry and the type and strength of interaction between the hydrogen donor and acceptor groups.[1] The strength of hydrogen bonds is substantially smaller than that of covalent bonds and results in structural flexibility and fluctuations of hydrogen-bonded systems which are essential for their chemical and/or biological function. On a microscopic level, the function of hydrogen-bonded systems is connected with vibrational motions of the hydrogen-bonded groups, a breaking and reformation of hydrogen bonds, and/or a transfer of hydrogen atoms or protons. Such processes cover a multitude of time scales, with many elementary events occurring in the ultrafast time domain between approximately 10 fs and several picoseconds.[2]

Vibrational spectroscopy can grasp local excitations of hydrogen-bonded groups and thus gives insight into local interactions and microscopic dynamics. For this reason, infrared and Raman spectroscopy have developed into important tools of hydrogen bond research. In steady-state vibrational spectroscopy, information on microscopic dynamics is derived from the line shapes of linear absorption or Raman spectra, i.e., from studies in the frequency domain. Most hydrogen-bonded systems, however, display highly complex and congested vibrational line shapes, pointing to a variety of interactions and line broadening mechanisms involved. This fact calls for spectroscopic tools allowing for a separation of the different interactions, which is frequently equivalent to a separation of time scales on which microscopic dynamics occur. Combinations of frequency- and time-domain spectroscopies, e.g., multidimensional nuclear magnetic resonance in the time domain longer than 1 ns, and in particular nonlinear vibrational spectroscopy in the ultrafast time domain from femtoseconds to picoseconds, have the potential to address the different microsopic processes separately.

In recent years, ultrafast nonlinear vibrational spectroscopy has developed into an important method to study hydrogen bonds. Photon-echo or, in general, coherent multidimensional spectroscopy using ultrashort pulses allows for a separation of different contributions to line broadening and for a measurement of microsopic coupling strengths between functional groups.[3] Quantum coherent vibrational wave packets which represent coherent microscopic motions of hydrogen-bonded groups can be excited by ultrashort optical pulses and followed in time by different types of pump−probe spectroscopies with

10.1021/cr020694p CCC: $48.50
Published on Web 03/18/2004

Erik T. J. Nibbering was born in 1965 in Zaandam, The Netherlands, and attended high school in Amsterdam. In 1983, he started his undergraduate studies in chemistry at the Vrije Universiteit in Amsterdam, where he received his diploma in physical chemistry in 1988. During his Ph.D. studies at the Rijksuniversiteit Groningen, under the direction of Professor Douwe A. Wiersma (1988–1993), he investigated femtosecond optical dephasing and solvation dynamics in liquids. After a two-year stay at the Laboratoire d'Optique Appliqueé – E.N.S.T.A. – École Polytechnique (Palaiseau, France) with Prof. Dr. André Mysyrowicz, where he investigated nonlinear propagation phenomena of intense femtosecond laser pulses, he joined the Max Born Institut für Nichtlineare Optik und Kurzzeitspektroskopie in Berlin, Germany, in 1995, under the supervision of Prof. Dr. Thomas Elsaesser, becoming project leader in 1997 and department head in 2003. His current interests encompass generation of ultrafast light pulses and ultrafast spectroscopy of condensed matter. His recent efforts include ultrafast dynamics of hydrogen bonds in liquids and solutions, proton-transfer reactions in the condensed phase, conformational changes of molecular switches, and structural dynamics of biomolecular systems.

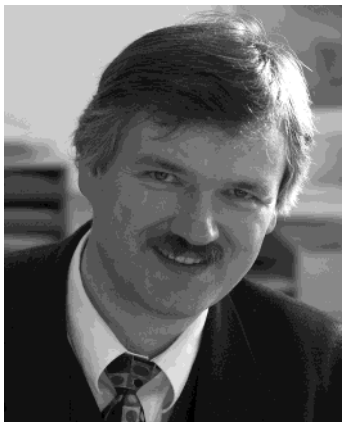

Thomas Elsaesser received a Ph.D. degree in physics in 1986 from the Technical University in Munich, Germany, for work on picosecond infrared spectroscopy. After working as a research assistant at the Physics Department of the Technical University of Munich and spending a postdoctoral period at AT&T Bell Laboratories, Holmdel, NJ, he became a director of the Max-Born-Institute in 1993, and a full professor of experimental physics at Humboldt University, Berlin, in 1994. He contributed to a broad range of research in ultrafast science, including technological work on femtosecond infrared generation and studies of elementary excitations in solids and liquids. A major part of his research is devoted to ultrafast photochemistry, in particular hydrogen-transfer processes, and to femtosecond vibrational spectroscopy of hydrogen bonds. For his work in ultrafast spectroscopy, he received the Rudolf-Kaiser-Prize in 1991, and the Otto-Klung-Prize for Physics in 1995.

individual pulses or pulse sequences. Such experiments also give insight into incoherent processes of population relaxation and energy transfer. In this article, we review recent progress in ultrafast vibrational spectroscopy of hydrogen bonds in liquids. We focus on the dynamics of coherent and incoherent

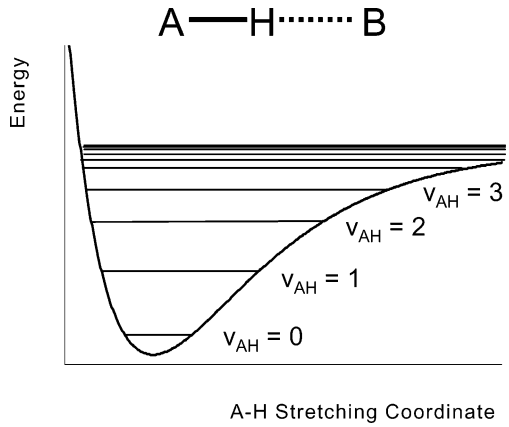

Figure 1. Schematic potential of the A−H stretching mode, showing the enhanced anharmonicity by formation of a hydrogen bond A−H···B.

vibrational excitations in the electronic ground state. For gas-phase studies of isolated hydrogen-bonded systems, we refer to recent overviews.[4−7] Hydrogen- and proton-transfer processes are beyond the scope of this article but have been reviewed elsewhere.[8,9]

The paper is organized as follows. In section 2, we discuss linear vibrational spectra and the mechanisms underlying their line shapes. This is followed by an introduction to nonlinear vibrational spectroscopy (section 3). The generation of ultrashort pulses in the mid-infrared and techniques of ultrafast vibrational spectroscopy are reviewed in section 4. We then discuss the coherent response of O−H/O−D stretching excitations, with the main emphasis on their vibrational dephasing and on coherent low-frequency motions (section 5). Chapter 6 is devoted to incoherent processes of vibrational energy relaxation and energy transfer. Conclusions and an outlook are presented in section 7.

2. Vibrational Spectra of Hydrogen Bonds

The present review concentrates on weak to medium-strong hydrogen bonds with a distinct hydrogen donor group A−H and an acceptor atom B, as schematically shown in Figure 1. In such cases, hydrogen bonding originates from an attractive interaction between the hydrogen donor group and the acceptor atom, leading to an H···B distance smaller than the van der Waals radii of the isolated H and B atoms. The underlying potential energy surface has been described by attractive long-range interactions, i.e., electrostatic, dispersion, and induction energies, and by a repulsive short-range exchange interaction at short distances.[10,11] The binding energy of weak to medium-strong hydrogen bonds of about 4−35 kJ/mol is equivalent to an energy per molecule between 350 and 3100 cm^{-1} and corresponds, for O—H···O bonds, to an O···O distance of 0.3−0.24 nm.

The attractive interaction between the hydrogen donor group and the acceptor atom modifies the molecular potential energy surface and has dramatic consequences for the vibrational spectra (for a brief review, see ref 12). In particular, the hydrogen stretching band of the hydrogen donor group undergoes a spectral shift to lower frequency and a substantial reshaping of its spectral envelope. More-

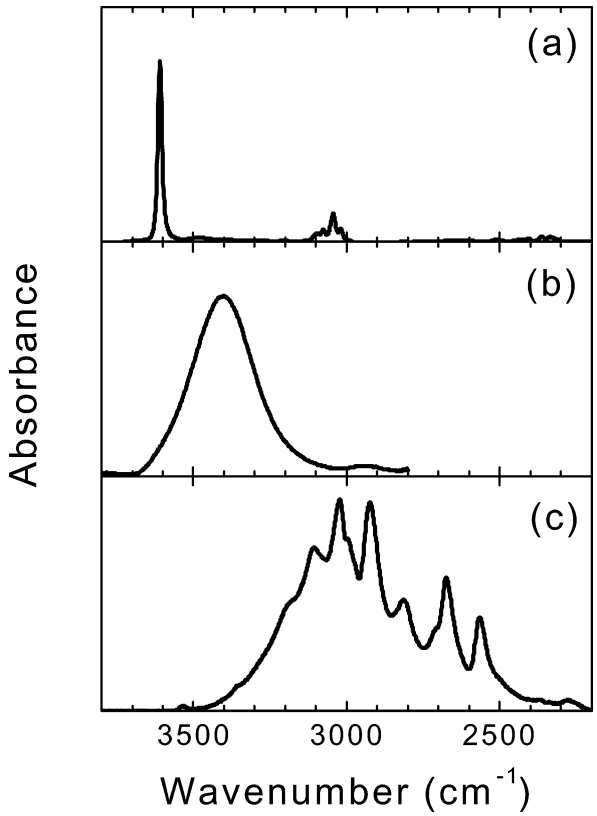

Figure 2. Infrared absorption spectra showing O−H stretching absorption bands of (a) the free O−H group of phenol in C_2Cl_4, (b) the weak hydrogen-bonded O−H group of HOD in D_2O, and (c) the medium-strong hydrogen-bonded O−H system in acetic acid dimer [$(CD_3COOH)_2$] dissolved in CCl_4.

over, new modes related to A···B motions occur at low frequencies of up to several hundreds of wavenumbers (cm^{-1}). Such drastic changes of the vibrational spectra have made vibrational spectroscopy one of the most powerful techniques to identify and analyze hydrogen bonds. In this section, we discuss the influence of hydrogen bonds on the linear vibrational spectra and introduce the relevant microscopic interactions between different oscillators. Nonlinear vibrational spectroscopy is reviewed in the following sections 3−6.

2.1. The Stretching Vibration of the Hydrogen Donor Group: Experimental Findings and Phenomenology

The red-shift of the stretching vibration reflects a decrease of the effective force constant of the hydrogen stretching oscillator. This basic effect has been studied most extensively for O−H stretching vibrations, in particular in O−H···O hydrogen bonds,[12−14] and representative examples are shown in Figure 2. Free O−H groups, e.g., in diluted phenol, give rise to an absorption band around 3600 cm^{-1} with a spectral width (full width at half-maximum) of 15−20 cm^{-1} (Figure 2a). The O−H stretching band of water, which forms an extended network of O−H···O hydrogen bonds, peaks at 3400 cm^{-1}. In Figure 2b, we show the O−H stretching band of HOD dissolved in D_2O, a model system for water with a single O−H group which has been studied in numerous experiments on ultrafast time scales. HOD:D_2O is classified as a weak hydrogen bond with an absorption maximum of the O−H stretching band at 3400 cm^{-1}, a bandwidth of 235 cm^{-1}, and an average hydrogen bond distance of 0.285 nm.[13,15,16]

In molecular systems forming medium-strong hydrogen bonds, the O−H stretching band has a typical position around 3000 cm^{-1}, a bandwidth exceeding 500 cm^{-1}, and shows often a fine structure ascribed to Fermi resonances with overtones and combination levels, as well as to Franck−Condon progressions due to anharmonic coupling to low-frequency hydrogen bond modes. The cyclic dimer of acetic acid has been regarded as a prototype for medium-strong hydrogen bonds since the landmark contribution by Marechal and Witkowski.[17] Apart from fundamental issues regarding hydrogen bonding, the cyclic acetic acid dimer is also a model system for hydrogen-bonded carboxylic side groups in glutamic and aspartic amino acids that play a key role in the structure and function of proteins. The O−H stretching band of cyclic acetic acid dimers dissolved in CCl_4 is shown in Figure 2c. Such bands have been the subject of detailed experimental[18−22] and theoretical work[17,21,23−25] for both the gas and liquid phases.

A substantial fraction of the observed red-shift of the hydrogen stretching band has been attributed to an increase of anharmonicity of the potential energy surface along the stretching coordinate. This effect lowers the $v = 1$ state of the stretching oscillator in energy, corresponding to a red-shift of the $v = 0 \rightarrow 1$ vibrational transition. The quantity $\Delta = \nu_{(v=2)} - 2\nu_{(v=1)}$ represents a direct measure of this so-called mechanical anharmonicity, where $\nu_{v=2}$ and $\nu_{v=1}$ are the spectral (peak) positions of the first overtone and the fundamental stretching band, respectively. Stretching oscillators of free O−H groups display a value of $\Delta \simeq -100$ cm^{-1}, which changes to minus several hundreds of cm^{-1} for hydrogen-bonded species.

Empirical relations between the peak position of O−H stretching bands and the length of the hydrogen bond, i.e., the O···O distance taken as a measure of bonding strength, have been derived from extensive spectroscopic data, in particular for O−H···O hydrogen bonds in crystals.[13,14,26] Such relations predict O···O distances between 0.26 and 0.3 nm for stretching frequencies between 2800 and 3500 cm^{-1}. This type of correlation may be useful for solid-state systems with a well-defined linear hydrogen-bonding geometry. Hydrogen-bonded liquids, however, are characterized by a multitude of binding geometries in which the O−H stretching frequency may depend on other geometric parameters and on interactions with the fluctuating environment as well (Figure 3, refs 27 and 28). For instance, recent molecular dynamics simulations of water and HOD in D_2O suggest that the degree of bending of the hydrogen bond has a strong influence on the spectral position.[27]

The strong broadening of the fundamental hydrogen stretching transition by up to approximately 500 cm^{-1} is usually connected with an enhancement of the spectrally integrated absorption, i.e., the oscilla-

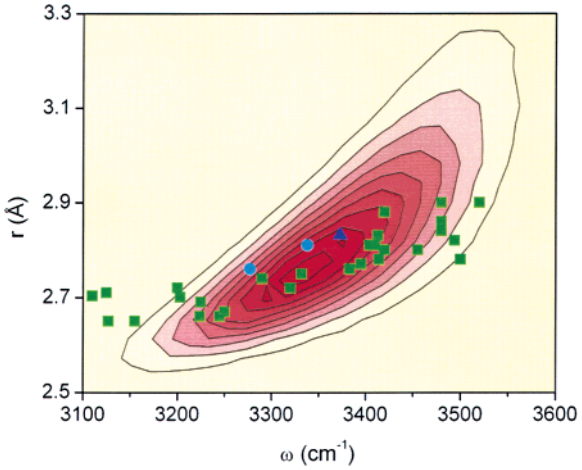

Figure 3. Joint probability distribution function of the O···O distance r vs frequency $\omega = 2\pi\nu_{OH}$ from the simulation by Lawrence and Skinner,[28] and average distance and frequency (closed squares) for a series of hydrogen-bonded solids.[13] Values for two forms of ice are shown as closed circles. The average values for the distance and frequency (for hydrogen-bonded HOD molecules) from the simulation are indicated by the closed triangle. Reproduced with permission from ref 28. Copyright 2003 American Institute of Physics.

tor strength of the transition, by a factor of up to 20. This behavior, together with the development of a peculiar spectral substructure, as one finds, e.g., in the spectra of carboxylic acid dimers (Figure 2c), represents a challenging problem of line shape theory, as different microscopic interactions of similar strength have to be considered. This will be discussed in section 2.3.

The stretching vibrations of other hydrogen donor groups, e.g., N−H or F−H groups, also display redshifts and spectral broadening upon formation of hydrogen bonds. Apart from the hydrogen stretching vibration, bending modes involving the A−H group and modes of the acceptor group show characteristic but smaller frequency shifts, a behavior that is beyond the scope of this review. A brief overview has been given in ref 12.

2.2. Low-Frequency Vibrations of Hydrogen Bonds

The attractive interaction between the hydrogen donor group and the acceptor moiety leads to the occurrence of new vibrational degrees of freedom, the so-called hydrogen bond modes. Such modes are connected with elongations changing the A···B distance and/or the relative orientation of the hydrogen-bonded groups. Thus, they provide direct insight into the structure of hydrogen bonds and into processes of bond formation and cleavage. As such modes are characterized by a high reduced mass of the oscillator and a small force constant determined by the comparably weak attractive interaction along the hydrogen bond, hydrogen bond modes occur at low frequencies in the range between about 50 and 300 cm^{-1}.

In liquids, the spectral range in which hydrogen bond modes occur is usually highly congested. Other low-frequency degrees of freedom such as librations as well as interaction-induced, e.g., dipole−induced dipole, absorption processes give rise to additional absorption and Raman bands that frequently overlap with the bands of the hydrogen bond modes. In addition, a substantial spread of vibrational frequencies occurs for liquids with a multitude of hydrogen-bonding geometries, resulting in a pronounced inhomogeneous broadening of the vibrational bands. The question to which extent motions along such low-frequency coordinates are over- or underdamped in a liquid environment has remained unresolved in most cases and led to substantial controversies in the literature.

Despite such problems, there is considerable knowledge on hydrogen bond modes, from both theory and experiment. Optical studies are based on techniques of infrared absorption and (depolarized) Raman spectroscopy[29] in the frequency domain and on Raman-induced Kerr effect spectroscopy in the time domain.[30] In addition, inelastic neutron scattering has provided insight into such modes.[31] The dielectric function at frequencies below 20 cm^{-1} has been investigated by microwave and time-domain terahertz spectroscopy.[32,33] In the following, we briefly discuss results for water as a prototype for an extended hydrogen-bonded network of molecules and for carboxylic acid dimers in nonpolar solution which represent a geometry with two coupled hydrogen bonds of well-defined symmetry.

Liquid H_2O displays a broad low-frequency Raman spectrum with distinct peaks around 60 and 175 cm^{-1} and a weaker broad band with a maximum around 440 cm^{-1} which extends up to approximately 1000 cm^{-1}.[30,34] The 60 cm^{-1} band has been attributed to a translational motion of the hydrogen-bonded molecules including some bending component, the 175 cm^{-1} band to a translational (stretching) motion of the hydrogen bond. The broad band with a maximum around 440 cm^{-1} has been assigned to different types of librations. The broad spectral envelopes have been interpreted in terms of rotational and translational diffusive motions of water molecules, without, however, reaching unambiguous conclusions. Ultrafast time-domain spectroscopies, in particular Raman-induced optical Kerr spectroscopy, give direct access to the microscopic molecular dynamics. For water, time constants of 0.4 and 1.2 ps have been measured for diffusive rotational reorientation.[30] It is important to note that the extended network of hydrogen bonds in water undergoes fluctuations on a time scale close to the vibrational periods of hydrogen bond modes. For instance, cleavage and re-formation of hydrogen bonds occur within a few picoseconds, directly affecting the vibrational reponse, in particular the damping of low-frequency motions.

Cyclic dimers of carboxylic acids, e.g., acetic acid (cf. Figure 2c), display a total of six intermonomer, i.e., hydrogen bond modes. Due to a C_2 symmetry axis perpendicular to the plane of the dimer, three of these modes are Raman active, whereas the other three are infrared active. The low-frequency Raman spectra of acetic acid dissolved in aprotic nonpolar solvents, where the cyclic dimer represents the predominant species,[35] and of pure acetic acid display three broad

bands at 55, 115, and 165 cm^{-1}.[36] Such bands have been attributed to an in-plane rotation of the two molecules against each other, an out-of-plane vibration of the two hydrogen bonds, and a stretching motion along the two hydrogen bonds of the cyclic dimer. For pure acetic acid, this assignment has been questioned as other dimer or oligomer geometries may exist and give rise to additional vibrational bands.[37] The low-frequency infrared spectrum in the gas phase consists of lines with maxima at 48.5 cm^{-1} attributed to a twist motion of the two molecules, at 56 cm^{-1}, an infrared bending motion of the dimer, and at 171 cm^{-1}, the antisymmetric dimer stretching mode.[38] The spectral envelope of the latter band shows signatures of Fermi resonances with combination tones of the other low-frequency modes.

2.3. Microsopic Interaction Mechanisms

Formation of a hydrogen bond changes the potential energy surface of the interacting molecules and thus results in the changes in the vibrational spectra discussed in the previous sections. In the following, we discuss the behavior of the stretching band of the hydrogen donor group, i.e., the red-shift of the $v = 0 \rightarrow 1$ vibrational transition and the pronounced changes of its spectral envelope.

Using the density matrix approach for describing the vibrational line shapes, the vibrational absorption coefficient for a $v = 0 \rightarrow 1$ transition is given by

$$\alpha(\omega) = \frac{2\pi}{3c\hbar n(\omega)V}\omega\left[1 - \exp\left(-\frac{\hbar\omega_0}{k_B T}\right)\right] \times \int_{-\infty}^{\infty} dt\, e^{-i(\omega-\omega_0)t} \langle \mathbf{M}(t)\mathbf{M}(0)\rangle \quad (1)$$

with

$$\langle \mathbf{M}(t)\mathbf{M}(0)\rangle = |\mu|^2 \langle \exp[-i \int_0^t \delta\omega(\tau)\, d\tau]\rangle \simeq \mu^2 \exp\left[-\frac{1}{2}\int_0^t\int_0^t \langle\delta\omega(\tau_1)\delta\omega(\tau_2)\rangle\, d\tau_1\, d\tau_2\right] \quad (2)$$

where μ is the dipole moment of the vibrational transition at frequency ω_0, and V and n represent the volume and the refractive index of the liquid sample, respectively.[39] The exponential prefactor in eq 1 accounts for a finite thermal population of the $v = 1$ level (k_B is the Boltzmann constant; T is the vibrational temperature). The vibrational line shape is essentially determined by the Fourier transform of the dipole moment correlation function $\langle \mathbf{M}(t)\mathbf{M}(0)\rangle$, which is taken as an ensemble average in the absence of an external perturbation. $\langle \mathbf{M}(t)\mathbf{M}(0)\rangle$ is related to the frequency fluctuation correlation function $\langle\delta\omega(\tau_1)\delta\omega(\tau_2)\rangle$ (eq 2). Here, $\delta\omega(\tau)$ represents the time-dependent fluctuation of the vibrational transition frequency ω_0.

A quantum mechanical calculation of the vibrational absorption coefficient requires a Hamiltonian including both the potential energy surface of the hydrogen-bonded molecules and the interactions with the surrounding solvent.[17,21,23,24,40] This requires an analysis of (i) the anharmonicities of the molecular potential along different vibrational coordinates, (ii) the Fermi resonances of vibrational levels shifted by hydrogen bond formation, (iii) couplings between different hydrogen bonds of identical or similar geometry, and (iv) the role of fluctuating forces in the liquid for phase relaxation, spectral diffusion, and the resulting line shapes.

(i) Weak and medium-strong hydrogen bonds are characterized by an enhanced but limited anharmonicity of vibrational modes, and thus a description in a normal-mode picture is appropriate in most cases. In general, the molecular potential energy function contains terms of third and higher order in a single vibrational coordinate, giving rise to a shift of the quantized vibrational levels, and higher terms containing mixed products of different vibrational coordinates, giving rise to both a shift of levels and a coupling of different modes.[10] The most elementary consequence of anharmonicity consists of a decreasing energy separation of vibrational states with increasing quantum number v which results, e.g., in a red-shift of the $v = 1 \rightarrow 2$ transition with respect to the $v = 0 \rightarrow 1$ fundamental (Figure 1). In the early literature, the red-shift of the fundamental $\nu_{OH} = 0 \rightarrow 1$ transition upon hydrogen bonding has been described in a semiempirical way by analytic potential energy functions invoking the hydrogen stretching coordinate and—as a second coordinate—the A$\cdots$B distance. The parameters of the potential energy functions have been adjusted to account for experimental results.[41−43] A more sophisticated approach starts from a highly accurate potential for the stretching mode of the isolated, i.e., non-interacting, molecule, including higher order terms in the stretching coordinate and in mixed products of coordinates (see, e.g., ref 44). The parameters of such potentials are adjusted by, e.g., fitting the gas-phase vibrational/rotational spectra. In a second step, an interaction Hamiltonian is introduced for the liquid.[27,28,45,46]

Anharmonic coupling of the high-frequency stretching motion to low-frequency hydrogen bond modes has been invoked to explain the strong broadening of the hydrogen stretching band upon formation of a hydrogen bond.[17,47] As the time scales of nuclear motions along the low- and high-frequency degrees of freedom differ by a factor on the order of 20, anharmonic coupling has been described in terms of a Born−Oppenheimer-like picture where the different states of the O−H stretching oscillator define a potential energy surface for the low-frequency modes (Figure 4). Dipole-allowed transitions from different levels of the low-frequency oscillator in the $\nu_{OH} = 0$ state to different low-frequency levels in the $\nu_{OH} = 1$ state lead to a progression of lines which is centered at the pure O−H stretching transition and displays a mutual line separation by one quantum of the low-frequency mode (Figure 5a). With increasing separation of the lines from the center of the progression, the absorption strength decreases because of decreasing Franck−Condon factors between the low-frequency levels involved. For each low-frequency mode coupling to an O−H stretching oscillator, an independent progression of lines occurs. It is obvious that this mechanism results in a strong broadening and/

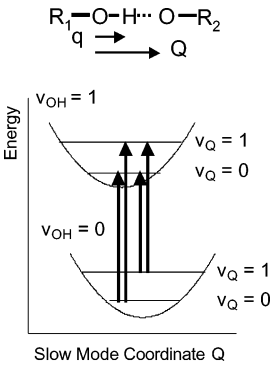

Figure 4. Potential energy surfaces for the hydrogen bond low-frequency mode in a single hydrogen bond, showing a displacement along the low-frequency coordinate Q as function of the quantum state of the O−H/O−D stretching mode, q. The O−H/O−D stretching transition is accompanied by changes in the low-frequency mode quantum state governed by Franck−Condon factors.

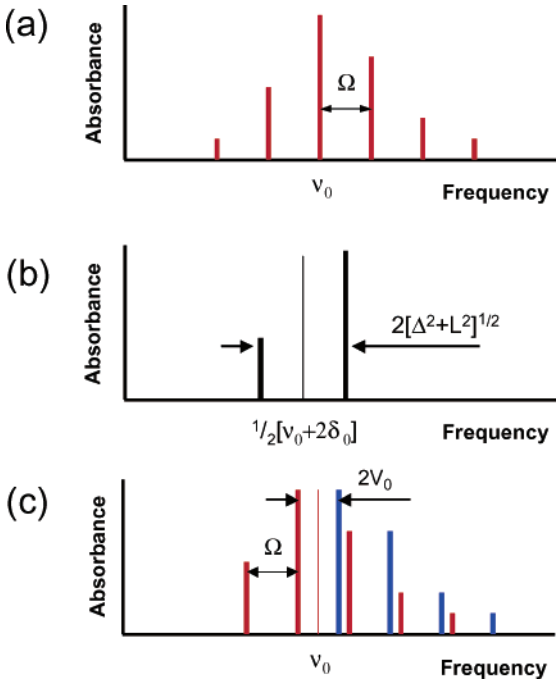

Figure 5. Stick spectra of the O−H/O−D stretching transition indicating different contributions. (a) A low-frequency mode anharmonically coupled to the O−H/O−D stretching mode in a single hydrogen bond leads to a Franck−Condon progression separated by the frequency of the low-frequency mode in the O−H/O−D stretching region. (b) Fermi resonance between the O−H/O−D stretching fundamental and the O−H/O−D first overtone leads to a line splitting governed by the Fermi coupling L and the energy mismatch Δ between the O−H/O−D fundamental frequency ν_0 and the bending overtone frequency $2\delta_0$. (c) Davydov coupling between two O−H or O−D groups in acetic acid dimer lead to an additional splitting $2V_0$, resulting in two Franck−Condon progressions in the low-frequency mode.

or spectral substructure of the overall O−H stretching band, even for a small number of absorption lines with large Franck−Condon factors.

(ii) Fermi resonances between the $\nu_{OH} = 1$ states of the stretching mode and overtones or combination bands of modes at lower frequency lead to an additional splitting of the O−H stretching transition into different components with a relative separation

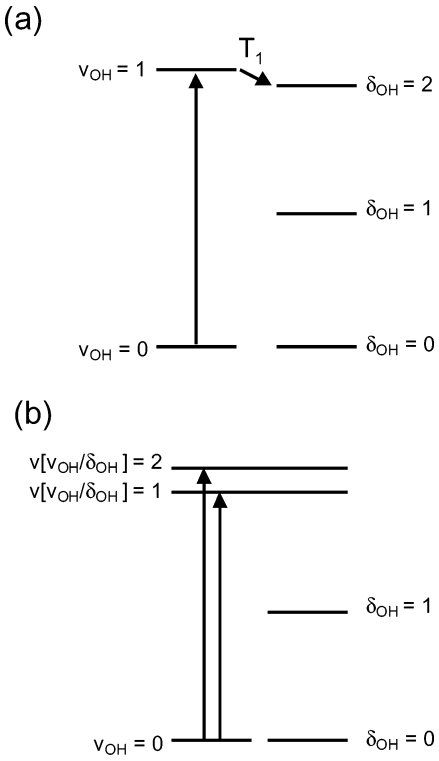

Figure 6. Fermi coupling in the weak (a) and strong limits (b) between the O−H/O−D stretching $\nu_{OH} = 1$ and the bending $\delta_{OH} = 2$ levels. In case (a), the weak Fermi resonance facilitates an efficient relaxation channel for energy redistribution, whereas case (b) explains the observation of additional transitions within the O−H/O−D stretching bands.

determined by twice the respective coupling (Figures 5b, 6). In numerous O−H···O hydrogen bonds, a Fermi resonance occurs between the $\delta_{OH} = 2$ bending level and the $\nu_{OH} = 1$ level, giving rise to the so-called Evans window in the O−H stretching band.[48] In addition to influencing the vibrational spectra, Fermi resonances play an important role for vibrational relaxation, as will be discussed in section 6.

(iii) In systems with multiple hydrogen bonds, excitonic or Davydov coupling can occur between different resonant oscillators.[17,49] Cyclic carboxylic acid dimers represent important model systems with coupled O−H stretching oscillators which have been analyzed in the pioneering work of Marechal and Witkowski.[17] In this approach, the $\nu_{OH} = 0$ states of the two O−H oscillators are considered degenerate, and the coupling comes into play whenever one of the oscillators is excited. The excitonic coupling V_0 leads to a splitting of the $\nu_{OH} = 1$ states by $2V_0$. Considering both anharmonic and excitonic coupling, the coupled system has been described by taking into account the C_2 symmetry axis of the cyclic dimer and introducing symmetrized vibrational coordinates $q_{g,u} = (1/\sqrt{(2)})(q_1 \pm q_2)$ and $Q_{i,g,u} = (1/\sqrt{(2)})(Q_{i,1} \pm Q_{i,2})$ for the stretching and the low-frequency modes i, respectively. The symmetry operator C_2 (in-plane rotation of the dimer by 180°) has the following properties: $C_2|\nu_g(q_g)\rangle = +|\nu_g(q_g)\rangle$ and $C_2|\nu_u(q_u)\rangle = (-1)^{\nu_u}|\nu_u(q_u)\rangle$ for the high-frequency O−H stretching mode, and $C_2|n_{i,g}(Q_{i,g})\rangle = +|n_{i,g}(Q_{i,g})\rangle$ and $C_2|n_{i,u}(Q_{i,u})\rangle = (-1)^{n_{i,u}}|n_{i,u}(Q_{i,u})\rangle$ for the low-frequency hydrogen bond mode (with $\nu_{g,u}$ and $n_{i,g,u}$ being the quantum numbers

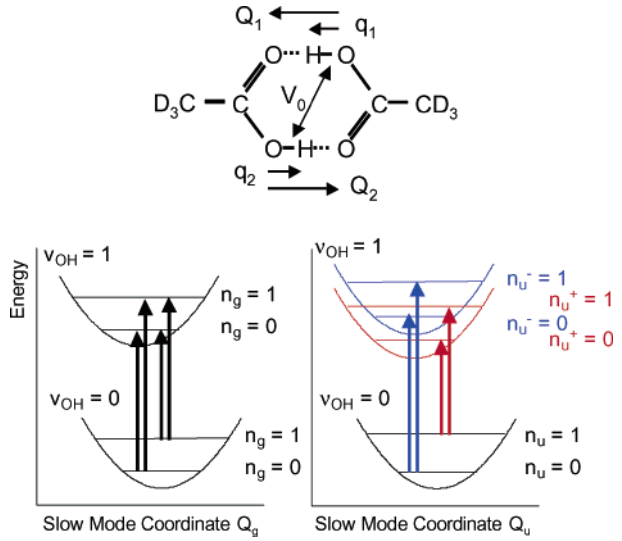

Figure 7. Schematic of the cyclic acetic acid dimer including high- ($q_{1,2}$) and low-frequency ($Q_{1,2}$) local mode coordinates. Schematic potential energy diagrams of low-frequency modes anharmonically coupled to the O−H/O−D stretching motion are shown in the lower part. The potential energy surfaces in the $\nu_{OH} = 0$ and $\nu_{OH} = 1$ states and the two lowest vibrational levels of the low-frequency mode are plotted versus symmetrized low-frequency coordinates Q_g and Q_u. For Q_u, the resonant (Davydov) splitting $2V_0$ in the $\nu_{OH} = 1$ state results in two series of vibrational transition lines (blue and red arrows) from the $n_u = 0$ and $n_u = 1$ levels.

of the $|\nu_{g,u}(q_{g,u})\rangle$ and $n_{i,g,u}(Q_{i,g,u})\rangle$ wave functions, respectively). Evaluating the dipole selection rules, one finds that transitions between $|\nu_u(q_u)\rangle$ states are infrared active, whereas transitions that alter the $|\nu_g(q_g)\rangle$ state are observed in the Raman band of the O−H stretching mode.[17,23,24] The $\nu_u = 1$ potential energy surface along the gerade $Q_{i,g}$ coordinate remains unaltered, whereas the excitonic coupling V_0 leads to a splitting of the $\nu_u = 1$ potential energy surface along the ungerade $Q_{i,u}$ coordinate by $2V_0$ (Figure 7). The resulting line shape consists of two different progressions between the $n_{i,u} = 0$ level of the $Q_{i,u}$ mode in the $\nu_u = 0$ state and the $n^-_{i,u}$ levels in the $\nu_u = 1$ state as well as between the $n_{i,u} = 1$ level in the $\nu_u = 0$ state and the $n^+_{i,u}$ levels in the $\nu_u = 1$ state (Figure 5c). Simultaneously, the number of quanta in the $Q_{i,g}$ mode can be changed when the system is excited to the $\nu_{OH} = 1$ state, introducing an additional degeneracy of the lines in the respective progression. It is important to note that an individual molecule displays only one of those progressions, depending on whether the $n_{i,Q} = 0$ or $n_{i,Q} = 1$ level in the $\nu_u = 0$ state is populated. In an ensemble of molecules at a sufficiently high vibrational temperature, both levels are populated; consequently, both series of lines contribute to the overall vibrational band.

(iv) In a liquid, a hydrogen bond is subject to the fluctuating forces exerted by the solvent bath, resulting in spectral diffusion and broadening of the vibrational transition lines. Overdamped intramolecular or solvent modes exert a fluctuating force on the O−H oscillators. Depending on the modulation strength and time scale, the spectra may vary between a distribution of transition frequencies corresponding to different hydrogen bond configurations (inhomogeneous broadening) or a single motionally narrowed transition (homogeneous broadening). There are different theoretical approaches to describe this problem. The first approach considers a direct interaction of the dipole moment of the hydrogen stretching mode with the local electric field exerted by the fluctuating solvent.[50,51] The second type of treatment introduces a stochastic motion of the low-frequency hydrogen bond modes that couple anharmonically to the fast stretching motion.[15,52,53] The stochastic low-frequency motions have been treated both as a classical overdamped[15] or underdamped[52] mode and as a stochastic quantized degree of freedom.[53] For a comparison of the different models, the reader is referred to a review by Henri-Rousseau and Blaise.[40] More recently, the influence of the solvent has been treated using molecular dynamics simulations.[27,28,45,46,54] Using a highly accurate Hamiltonian for the isolated molecule and a Hamiltonian containing Lennard-Jones and Coulomb terms for the intermolecular interactions, the renormalization of the vibrational quantum states in the fluctuating solvent has been calculated in a self-consistent way for the system HOD in D_2O.

It is important to note that the interactions (i)−(iii) transform the hydrogen stretching oscillator into a vibrational multilevel system with a multitude of transition lines. The interaction with the liquid (mechanism (iv)) leads to a substantial broadening of the individual lines and thus washes out any fine structures in the spectra. As a result, a quantitative line shape analysis of linear vibrational spectra in the liquid-phase spectra has remained difficult. A quantitative and unambiguous theoretical calculation of spectra is hampered by the similar strengths of the interaction mechanisms (i)−(iv) and/or the large number of molecular parameters required. As a result, linear vibrational spectroscopy does not allow for a separation of the different coupling and broadening mechanisms. It is a particular strength of nonlinear vibrational spectroscopy in the ultrafast time domain to overcome this drawback and to provide highly specific information on the different couplings by separating them in the nonlinear time-resolved response.

3. Nonlinear Vibrational Spectroscopy of O–H/O–D Stretching Modes

The subject of this section is to indicate which features are expected to play a role in nonlinear vibrational spectroscopy, and to give a description of the nonlinear signals in the framework of perturbation theory.

3.1. Nonlinear O–H/O–D Stretching Excitations

Ultrafast vibrational spectroscopy not only enables the determination of real-time dynamics of vibrational states, but through the bandwidth of the laser pulses it also has the potential to excite a collection of the vibrational levels in a coherent superposition and to follow the coherent nuclear motions in real time. The multilevel character as well as the coherent

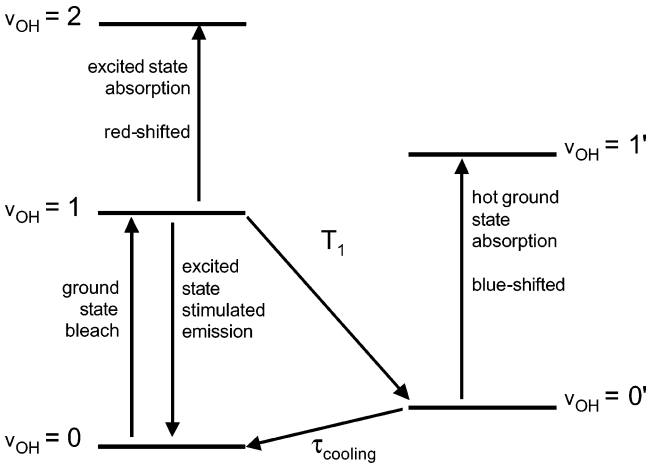

Figure 8. Level structure implementing the $v_{OH} = 0$, $v_{OH} = 1$, and $v_{OH} = 2$ states of the O−H/O−D stretching mode, as well as two levels of the hot molecule that shows up when the $v_{OH} = 1$ state decays.

nature of O−H/O−D stretching excitations in hydrogen bonds thus have to be taken into account in the interpretation of the observed nonlinear signals.

Nonlinear vibrational spectroscopy can be treated in a perturbative manner, similar to nonlinear electronic spectroscopy. In contrast with the latter, vibrational spectroscopy always has to consider the multilevel nature of the vibrational systems (Figures 4-7). As a consequence of anharmonicity, the $v_{OH} = 0 \rightarrow 1$ and the $v_{OH} = 1 \rightarrow 2$ transitions are centered at different spectral positions, separated by the anharmonic shift of up to several hundreds of cm^{-1}. Since these transitions have a spectral broadening that is of the same order of magnitude, an ultrafast laser pulse, typically with a bandwidth of 100−200 cm^{-1}, is likely to have spectral components that may interact with either transition. In a theoretical treatment of nonlinear vibrational spectroscopy, one thus has to take into account Liouville space pathways through either of these states. For instance, upon excitation of the $v_{OH} = 0 \rightarrow 1$ O−H/O−D stretching transition in spectrally resolved pump−probe spectroscopy, one observes the $v_{OH} = 0 \rightarrow 1$ O−H/O−D ground-state bleaching and $v_{OH} = 1 \rightarrow 0$ stimulated emission, both leading to a decrease of absorption at the position of the O−H/O−D stretching band observed in the linear absorption spectrum (Figure 8). In addition, a transient red-shifted absorption occurs on the $v_{OH} = 1 \rightarrow 2$ excited-state transition. This spectral feature decays upon population relaxation of the $v_{OH} = 1$ state.

From a large collection of experimental work on the transient spectra of O−H/O−D stretching bands which will be discussed in detail in section 6, the general conclusion has been drawn that the $v_{OH} = 1$ state does not decay directly back to the $v_{OH} = 0$ state upon population (T_1) relaxation by directly dissipating the vibrational excitation energy to the surrounding solvent modes. Instead, a hot ground-state $v_{OH} = 0'$ is reached in which the O−H stretching oscillator is not excited but other modes of the hydrogen-bonded system, e.g., O−H/O−D bending and low-frequency hydrogen bond vibrations, contain vibrational excess energy. The $v_{OH} = 0'$ state shows, through anharmonic coupling with these excited modes, a blue-shifted transient $v_{OH} = 0' \rightarrow 1'$ absorption that contributes to the nonlinear signal.

The anharmonic coupling of the stretching and the low-frequency hydrogen bond modes allows for the preparation of a quantum-coherent superposition of several low-frequency levels by exciting the stretching motion with a broadband femtosecond pulse. For underdamped low-frequency modes, this results in wave packet motions of the low-frequency mode in the $v_{OH} = 0$ and $v_{OH} = 1$ states, contributing quantum beats to the nonlinear signals. We discuss recent studies of such wave packet motions in section 5.2.

Fermi resonances of the $v_{OH} = 1$ state with combination or overtone states also play a role for the nonlinear signals. When the Fermi resonance is weak, the bend overtone is often assumed to be a major channel for the vibrational energy redistribution by which the O−H/O−D stretching excited-state population can relax (see section 6). Moreover, when the Fermi resonance interaction is strong, the resulting coupled states split, and coherent excitation of these split states will also result in quantum beats in the nonlinear signals. Finally, for multiple hydrogen-bonded systems with spectrally overlapping O−H/O−D stretching transitions, excitonic (Davydov) coupling between the O−H/O−D stretching oscillators results in a modification of the level structure, and coherent excitation leads to quantum beats or macroscopic polarization beats in nonlinear spectroscopy. We will discuss in section 5.3 recent results in photon-echo spectroscopy on the cyclic acetic acid dimer where these effects potentially play a role.

3.2. Theoretical Description of Nonlinear Vibrational Spectroscopy

The theoretical treatment of nonlinear vibrational spectroscopy presented here relies on perturbation theory and has been worked out before in the context of nonlinear electronic spectroscopy by Mukamel.[55] The extension to nonlinear vibrational spectroscopy has been described in a recent review by Hamm and Hochstrasser.[56] From a microscopic point of view, vibrational dephasing was first described by Oxtoby.[57−59] We also note the theoretical work by Bratos and co-workers on infrared pump−probe spectroscopy of water,[60−62] and by Loring and co-workers on vibrational photon echoes.[63−66] We give here only that part of the theory necessary to understand the essentials of nonlinear vibrational response in hydrogen bonds.

Double-sided Feynman diagrams are a standard means of depicting the possible Liouville pathways that may contribute to the total signal. In nonlinear electronic spectroscopy, only four diagrams suffice for the description of pump−probe and photon-echo spectroscopy.[55] Due to the multilevel structure of hydrogen-bonded O−H/O−D stretching vibrations, 10 different diagrams in total have to be taken into account (Figure 9).[56,67] Diagrams I−IV are denoted as rephasing pathways due to the time reversal of the system evolution in period t_3 after a coherence period t_1 and a population period t_2. Diagrams V−X, on the other hand, do not cause a rephasing. Dia-

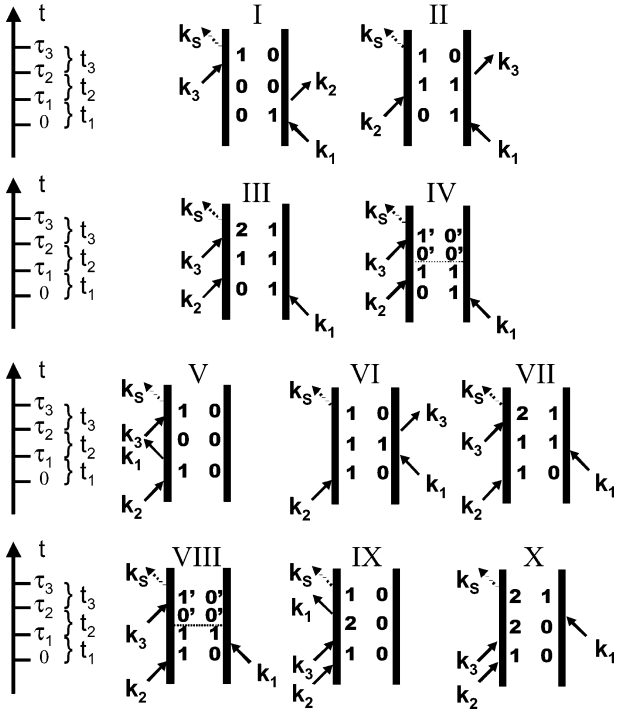

Figure 9. Double-sided Feynman diagrams that have to be considered in nonlinear infrared experiments. Diagrams I−IV describe echo-generating (rephasing) Liouville space pathways, while diagrams V−X symbolize pathways that do not generate an echo (non-rephasing). Diagrams I, II, V, and VI are diagrams for a two-level system. Diagrams III, VII, IX, and X are also contributing in a three-level system with excited-state absorption from $v_{OH} = 1$ to $v_{OH} = 2$. Diagrams IV and VIII take the process of relaxation to a hot ground state into account. This process is indicated by a horizontal dashed line.

grams III, VI, IX, and X have to be implemented for a vibrational ladder system. Diagrams II, III, VI, and VII diminish in importance upon T_1 (population) relaxation. Diagrams IV and VIII have to be implemented due to the five-level nature of O−H/O−D stretching vibrations, including the states $v_{OH} = 0$, 1, 2, 0′, and 1′.[67] The intricacies of conservation or decay of phase coherence upon T_1 relaxation will be discussed in section 5.1.2.

The material response functions R_I−R_X describe the following system evolutions:

$$\begin{aligned}
R_I &= \langle \mu_{01}(\tau_3)\mu_{10}(\tau_2)\rho_{00}\mu_{01}(0)\mu_{10}(\tau_1)\rangle \\
R_{II} &= \langle \mu_{01}(\tau_3)\mu_{10}(\tau_1)\rho_{00}\mu_{01}(0)\mu_{10}(\tau_2)\rangle \\
R_{III} &= \langle \mu_{12}(\tau_3)\mu_{21}(\tau_2)\mu_{10}(\tau_1)\rho_{00}\mu_{01}(0)\rangle \\
R_{IV} &= \langle \mu_{0'1'}(\tau_3)\mu_{1'0'}(\tau_2)\mu_{10}(\tau_1)\rho_{00}\mu_{01}(0)\rangle \\
R_V &= \langle \mu_{01}(\tau_3)\mu_{10}(\tau_2)\mu_{01}(\tau_1)\mu_{10}(0)\rho_{00}\rangle \\
R_{VI} &= \langle \mu_{01}(\tau_3)\mu_{10}(0)\rho_{00}\mu_{01}(\tau_1)\mu_{10}(\tau_2)\rangle \\
R_{VII} &= \langle \mu_{12}(\tau_3)\mu_{21}(\tau_2)\mu_{10}(0)\rho_{00}\mu_{01}(\tau_1)\rangle \\
R_{VIII} &= \langle \mu_{0'1'}(\tau_3)\mu_{1'0'}(\tau_2)\mu_{10}(0)\rho_{00}\mu_{01}(\tau_1)\rangle \\
R_{IX} &= \langle \mu_{01}(\tau_3)\mu_{12}(\tau_2)\mu_{21}(\tau_1)\mu_{10}(0)\rho_{00}\rangle \\
R_X &= \langle \mu_{12}(\tau_3)\mu_{21}(\tau_1)\mu_{10}(0)\rho_{00}\mu_{01}(\tau_2)\rangle
\end{aligned} \tag{3}$$

Here, ρ_{00} represents the equilibrium density matrix of the system and $\mu_{ij}(\tau)$ the transition dipole interaction between levels i and j at time τ. Typically it is assumed that these four-time-point correlation functions can be approximated by products of two-time-point correlation functions with the help of the cumulant expansion.[55,68] The nonlinear response functions then become

$$\begin{aligned}
R_I &= |\mu_{10}|^4\, e^{i\omega_{10}(t_3-t_1)} \times \\
&\quad \exp[-g(t_1) + g(t_2) - g(t_3) - g(t_2+t_1) - \\
&\qquad g(t_3+t_2) + g(t_1+t_2+t_3)] \\
R_{II} &= R_I\, e^{-t_2/T_1} \\
R_{III} &= -|\mu_{10}|^2\, |\mu_{21}|^2\, e^{i\alpha t_3}\, e^{i\omega_{10}(t_3-t_1)}\, e^{-t_2/T_1} \times \\
&\quad \exp[-g(t_1) + g(t_2) - g(t_3) - g(t_2+t_1) - \\
&\qquad g(t_3+t_2) + g(t_1+t_2+t_3)] \\
R_{IV}^{uncorr} &= -(1 - e^{-t_2/T_1})\, |\mu_{10}|^2\, |\mu_{1'0'}|^2\, e^{i\omega_{10}(t_3-t_1)}\, e^{i\Delta' t_3} \times \\
&\qquad \exp[-g(t_1) - g(t_3)] \\
R_{IV}^{corr} &= -(1 - e^{-t_2/T_1})\, |\mu_{10}|^2\, |\mu_{1'0'}|^2\, e^{i\omega_{10}(t_3-t_1)}\, e^{i\Delta' t_3} \times \\
&\quad \exp[-g(t_1) + g(t_2) - g(t_3) - g(t_1+t_2) - \\
&\qquad g(t_2+t_3) + g(t_1+t_2+t_3)] \\
R_V &= |\mu_{10}|^4\, e^{i\omega_{10}(t_3-t_1)} \times \\
&\quad \exp[-g(t_1) - g(t_2) - g(t_3) + g(t_2+t_1) + \\
&\qquad g(t_3+t_2) - g(t_1+t_2+t_3)] \\
R_{VI} &= R_V\, e^{-t_2/T_1} \\
R_{VII} &= -|\mu_{10}|^2\, |\mu_{21}|^2\, e^{i\alpha t_3}\, e^{i\omega_{10}(t_3+t_1)}\, e^{-t_2/T_1} \times \\
&\quad \exp[-g(t_3) - g(t_2) - g(t_1) + g(t_1+t_2) + \\
&\qquad g(t_2+t_3) - g(t_1+t_2+t_3)] \\
R_{VIII}^{uncorr} &= -(1 - e^{-t_2/T_1})\, |\mu_{10}|^2\, |\mu_{1'0'}|^2\, e^{i\omega_{10}(t_3+t_1)} \times \\
&\qquad e^{i\Delta' t_3} \exp[-g(t_1) - g(t_3)] \\
R_{VIII}^{corr} &= -(1 - e^{-t_2/T_1})\, |\mu_{10}|^2\, |\mu_{1'0'}|^2\, e^{i\omega_{10}(t_3+t_1)}\, e^{i\Delta' t_3} \times \\
&\quad \exp[-g(t_1) - g(t_2) - g(t_3) + g(t_1+t_2) + \\
&\qquad g(t_2+t_3) - g(t_1+t_2+t_3)] \\
R_{IX} &= |\mu_{10}|^2\, |\mu_{21}|^2\, e^{i\omega_{10}(t_3+2t_2+t_1)}\, e^{i\alpha t_2} \times \\
&\quad \exp[g(t_1) - g(t_2) + g(t_3) - g(t_1+t_2) - \\
&\qquad g(t_2+t_3) - g(t_1+t_2+t_3)] \\
R_X &= -|\mu_{10}|^2\, |\mu_{21}|^2\, e^{i\omega_{10}(t_3+2t_2+t_1)}\, e^{i\alpha(t_3+t_2)} \times \\
&\quad \exp[g(t_1) - g(t_2) + g(t_3) - g(t_2+t_1) - \\
&\qquad g(t_3+t_2) - g(t_1+t_2+t_3)]
\end{aligned} \tag{4}$$

with the line shape function $g(t)$[55] given by

$$g(t) = \int_0^t d\tau' \int_0^{\tau'} d\tau''\, C(\tau'') \tag{5}$$

and the transition frequency fluctuation correlation function $C(t)$,

$$C(t) = \langle \delta\omega(t)\, \delta\omega(0) \rangle \quad (6)$$

Here, ω_{ij} is the transition frequency between levels i and j, $\alpha = -\Delta$ is the anharmonicity of the oscillator, and Δ' is the shift between the fundamental transitions of the cold ($v_{OH} = 0 \rightarrow 1$) and hot ($v_{OH} = 0' \rightarrow 1'$) molecule; T_1 is the population lifetime of the $v = 1$ state. The third-order nonlinear polarization $P(t)$ that governs the nonlinear signals is a function of the material response functions $R_I - R_X$ and of the applied laser fields, $E_i(t)$:

$$P^{(3)}(t) = \int_0^\infty \mathrm{d}t_3 \int_0^\infty \mathrm{d}t_2 \int_0^\infty \mathrm{d}t_1 \sum_{i=I}^{X} R_i(t_1,t_2,t_3) \times E_3(t - t_3)\, \mathrm{e}^{-i\omega(t-t_3)} E_2(t - t_3 - t_2)\, \mathrm{e}^{-i\omega(t-t_3-t_2)} \times E_1^*(t - t_3 - t_2 - t_1)\, \mathrm{e}^{i\omega(t-t_3-t_2-t_1)} \quad (7)$$

In the case of ultrashort pulses well-separated in time, only diagrams I−IV contribute to the signals. In this case, the laser pulse delays τ (between pulses 1 and 2) and T (between pulses 2 and 3) equal the laser field interaction times; i.e., $t_1 = \tau$, $t_2 = T$, and $t_3 = t$. Diagrams V−X describe coherent coupling effects during pulse overlap and, in addition, when pump and probe pulses are well-separated in time, describe the perturbed free induction decay that leads to signals at negative pulse delays in frequency-resolved pump−probe spectroscopy.[69,70]

An important goal in performing coherent nonlinear spectroscopic experiments is to obtain the frequency fluctuation correlation $C(t)$, since this quantity gives direct insight into the interactions that the system under study has with the fluctuating environment. We come back to this important function, and what we may learn from it, when we discuss recent photon-echo and hole-burning experiments on hydrogen bonds.

Finally, we note that we have so far treated the O−H/O−D stretching vibration as consisting of discrete quantum states with quantum number v_{OH}, combined with a broadening mechanism due to the fluctuating surrounding solvent. When incorporating the multilevel structure due to anharmonic coupling with hydrogen bond low-frequency modes, or due to Fermi resonances and Davydov coupling, one can resort to a summing-over-states approach.[55] As will be discussed in section 5.2, the anharmonically coupled low-frequency modes have frequencies comparable to the laser bandwidth, and to $k_B T$. Wave packet motions thus are due to coherent superposition of a limited number of low-frequency mode eigenstates. As a result, semiclassical approaches, such as the Brownian oscillator model, are less appropriate in the description of the experiments. In contrast, interaction with the fluctuating surrounding solvent, responsible for homogeneous and inhomogeneous broadening and spectral diffusion, can be described using strongly overdamped solvent modes that may be implemented using either Kubo's stochastic modulation model[68] or Mukamel's Brownian oscillator model.[55]

4. Techniques of Ultrafast Vibrational Spectroscopy

4.1. Ultrashort Infrared Pulses

Progress in ultrafast vibrational spectroscopy is closely linked to developing sources for ultrashort pulses in the mid- to far-infrared spectral range. So far, spectroscopic studies of hydrogen bonds have mainly concentrated on the wavelength range between 2.5 and 20 μm (500−4000 cm^{-1}). Resonant nonlinear excitation of vibrational transitions requires pulses with energies in the microjoule range. Generation of such pulses is mainly based on techniques of nonlinear optical frequency mixing. To a much lesser extent, pulses from free electron lasers have been applied. In the following, we discuss pulse generation in this mid-infrared spectral range.

Parametric amplification, difference frequency mixing, and optical rectification in solid-state materials with a nonvanishing second-order nonlinearity $\chi^{(2)}$ have been applied for generating mid-infrared pulses.[71,72] In such processes, pulses at center frequencies ω_p, ω_s, and ω_i, with $\omega_i < \omega_s < \omega_p$ (p = pump, s = signal, i = idler), interact with each other in the nonlinear medium.[71] Energy conservation requires $\omega_p = \omega_s + \omega_i$. In parametric generation and amplification, an intense input pulse at ω_p generates/amplifies pulses at ω_s and ω_i. In difference frequency mixing, pulses at $\omega_i = \omega_p - \omega_s$ are generated from two input pulses at ω_p and ω_s. Optical rectification represents a special case of difference frequency mixing where $\omega_p \simeq \omega_s$ and ω_i is on the order of $\Delta\omega_{p,s}$, the spectral bandwidth of the input pulses.

The phase relationship between the electric fields of the three interacting pulses is determined by the phase-matching condition $\boldsymbol{k}_p = \boldsymbol{k}_s + \boldsymbol{k}_i$, where $\boldsymbol{k}_{p,s,i} = n_{p,s,i}(\omega_{p,s,i}/c)$ are the respective wavevectors. This phase-matching condition can be fulfilled by adjusting the refractive indices $n_{p,s,i}$ in birefringent nonlinear media (c is the vacuum velocity of light).[71] Frequency tuning of the generated pulses is achieved by changing the phase-matching angle through rotation of the nonlinear crystal or variation of its temperature. Even for phase-matched parametric frequency conversion, there is a substantial mismatch of the group velocities of the three interacting pulses. The different group velocities limit the effective interaction length in the nonlinear medium and determine the minimum pulse duration achieved.[73] In most sources for femtosecond infrared pulses, the peak intensities of the input pulses are between 1 GW/cm^2 and 1 TW/cm^2, resulting in an energy conversion efficiency into the infrared between several 10^{-5} and several percent.

There is a limited number of birefringent nonlinear materials suitable for phase-matched parametric frequency mixing in the mid-infrared, the main issues being a sufficiently broad range of infrared transparency and high crystal quality, e.g., optical homogeneity and the absence of scattering centers.[72] For idler wavelengths of up to 5 μm, bulk and

periodically poled $LiNbO_3$, $LiIO_3$, $KNbO_3$, β-barium borate (BBO), and $KTiOPO_4$ (KTP) have been used. $AgGaS_2$ represents a standard material for wavelengths up to 12 μm, whereas $AgGaSe_2$ and GaSe allow for parametric mixing at even longer wavelengths up to approximately 20 μm. Data of nonlinear materials have been summarized in ref 72.

There are different schemes for generating pulses at megahertz and kilohertz repetition rates:

(i) Femtosecond mid-infrared pulses at megahertz repetition rates have been derived from near-infrared pulses which were generated with average powers on the order of 100 mW in self-modelocked Ti:sapphire oscillators or in optical parametric oscillators (OPOs) synchronously pumped by mode-locked Ti:sapphire lasers. In a conceptually simple and reliable approach, two frequency components from a single 800 nm pulse of 10−20 fs duration and $\Delta\lambda = 100$ nm (fwhm) bandwidth drive the mixing process. Using the second-order nonlinearity of a GaAs surface for non-phase-matched frequency mixing,[74,75] a very broad infrared spectrum is generated with low conversion efficiency. Substantially higher mid-infrared average powers in the microwatt range have been achieved by phase-matched difference frequency mixing in thin GaSe crystals, driven by 10−20 fs pulses at an 80 MHz or—when generated in a cavity-dumped oscillator—a 2 MHz repetition rate.[76,77] The finite acceptance bandwidth of the phase-matching process results in a selection of input wavelengths contributing to the nonlinear process and, consequently, a well-defined spectral envelope of the mid-infrared pulses which are tunable between 7 and 20 μm. For crystals as thin as 30 μm, wavelength components up to 100 μm have been generated.[78] Depending on the crystal thickness and the wavelength position, the pulse durations are between 30 and 300 fs.

Optical parametric oscillators (OPOs) provide femtosecond pulse trains with average powers of up to several hundred milliwatts and a tuning range of the signal pulses between about 1 and 2 μm, depending on the specific nonlinear material.[79−81] For the corresponding idler pulses, tunability between about 2 and 5 μm has been demonstrated with lower average powers. The duration of signal and idler pulses was between 100 and 500 fs, strongly depending on the wavelength position. Extension of the tuning range to wavelengths up to 18 μm has been achieved by difference frequency mixing of the signal and idler pulses from the OPO in an additional nonlinear crystal placed outside the resonator of the OPO.[82−84]

A complete characterization of the mid-infrared pulses requires measurement of their time-dependent electric field which is possible by electrooptic sampling, a technique that was originally developed for the far-infrared around 300 μm.[85] The infrared pulse induces a change of the refractive index in a birefringent electrooptic crystal, e.g., ZnTe, which is proportional to its momentary electric field and monitored through the polarization rotation of an ultrashort probe pulse. Changing the delay between infrared and probe pulse, the time-dependent electric field of the infrared pulse is determined. For a quantitative measurement, the probe pulse has to be short compared to the period of the infrared field, and group velocity dispersion in the electrooptic crystal has to be limited. Using 10 fs pulses at 800 nm and ZnTe crystals of typically 10 μm thickness, infrared pulses up to a wavelength of about 7 μm have been characterized.[85] Other techniques allowing a measurement of the relative optical phase of the pulses, e.g., frequency-resolved optical gating (FROG), have also been applied for characterizing mid-infrared pulses.[86]

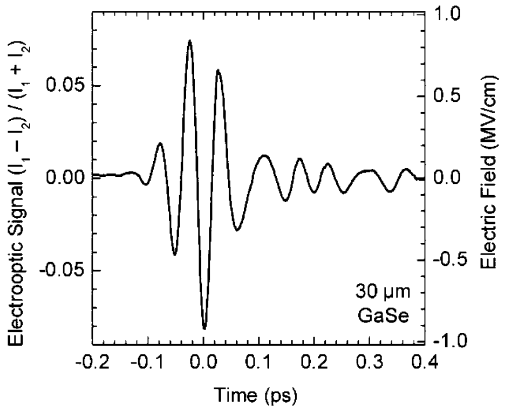

Figure 10. Femtosecond infrared pulse generated by optical rectification in a 30 μm GaSe crystal. The electric field of the pulse measured by electrooptic sampling is plotted as a function of time. The maximum field amplitude is approximately 1 MV/cm, the center wavelength 15 μm (frequency 670 cm^{-1} [95]).

(ii) Intense near-infrared pulses generated in regenerative Ti:sapphire amplifiers at kilohertz repetition rates have been used for pumping a variety of parametric conversion schemes. For a recent overview, the reader is referred to ref 87. In the wavelength range from 2.5 to approximately 10 μm, pulses of 50−150 fs duration and energies up to 20 μJ are generated routinely in a number of conversion schemes.[88−90] In addition, different techniques for generating phase-shaped mid-infrared pulses have been proposed and demonstrated.[91−94] Very recently, infrared pulses with an electric field amplitude up to megavolts per centimeter have been generated between 10 and 20 μm by difference frequency mixing of spectral components of an amplified 25 fs pulse in a thin GaSe crystal.[95] Such pulses at a repetition rate of 1 kHz have been characterized by electrooptic sampling with 12 fs pulses from the 75 MHz repetition rate oscillator of the laser system using a novel electronic gating technique. As an example, the time-dependent electric field of a pulse centered at 15 μm is plotted in Figure 10, giving a width of the intensity envelope (fwhm, pulse duration) of approximately 50 fs.

In recent years, infrared generation in free electron lasers (FELs) has received increasing interest.[96] At wavelengths between 5 and 10 μm, macropulses consisting of a sequence of 0.5 ps micropulses and microjoule energies per micropulse have been produced using short electron bunches from a linear accelerator. The wide tuning range and the microjoule energies per micropulse make FELs attractive for spectroscopic studies. For studies of liquids,

however, averaging of the signals over the macropulse and heating of the samples due to repetitive excitation are experimental limitations. Synchronization of FEL pulses with pulses from an external laser source, e.g., for two-color pump−probe experiments, represents another issue. Recently, synchronization of a FEL and a mode-locked Ti:sapphire laser with a jitter of about 400 fs has been demonstrated.[97]

4.2. Spectroscopic Techniques

Ultrafast vibrational spectroscopy is, in principle, based on the same nonlinear time-resolving methods as studies of electronic excitations. The infrared absorption and Raman cross sections, however, are several orders of magnitude smaller than those of electronic transitions, and thus, intense excitation pulses are required to generate nonlinear vibrational excitations. For this reason, most experiments make use of amplified femtosecond pulses with infrared pulse energies in the microjoule range.

Pump−probe techniques have widely been applied to study ultrafast vibrational dynamics. Here, an intense pump pulse generates a nonlinear vibrational excitation, i.e., a polarization on the vibrational transition and a population change of the optically coupled vibrational levels. The resulting change of transmission is probed by much weaker pulses at the same or a different spectral position and measured as a function of the time delay between pump and probe. The probe is usually detected in a time-integrating way, either by integrating over the probe spectrum (Figure 11a) or by dispersing the probe pulse and detecting it in a spectrally resolved way (Figure 11b). Measurements with a spectrally dispersed probe provide transient spectra and allow one, e.g., to follow the evolution of spectral holes or other features in the transient band. Changes of vibrational population induced by an infrared pump pulse have been monitored also by spontaneous anti-Stokes Raman scattering of a visible or near-infrared probe pulse or by fluorescence generated by a second probe-induced vibronic excitation.[98,99] Such probing techniques allow for a selective measurement of the time-dependent population of excited vibrational states. However, detection of the very weak Raman signals is a major experimental challenge.

In terms of nonlinear optics, pump−probe spectroscopy is third-order in the electric field. A third-order polarization is generated in the sample by two interactions with the pump and one interaction with the probe field. This polarization is detected through the field radiated in the propagation direction of the probe, and the two electric fields interfere on the detector. It is obvious from this description that both transient polarizations and population changes, i.e., real and imaginary parts of the nonlinear susceptibility, contribute to the pump−probe signal. In the slowly varying envelope approximation, i.e., for a pulse envelope varying slowly compared to the carrier frequency of the optical field, the spectrally integrated absorption change $\Delta\alpha(\omega_{pr})$ measured by a probe pulse with center frequency ω_{pr} signal is given by[55,100]

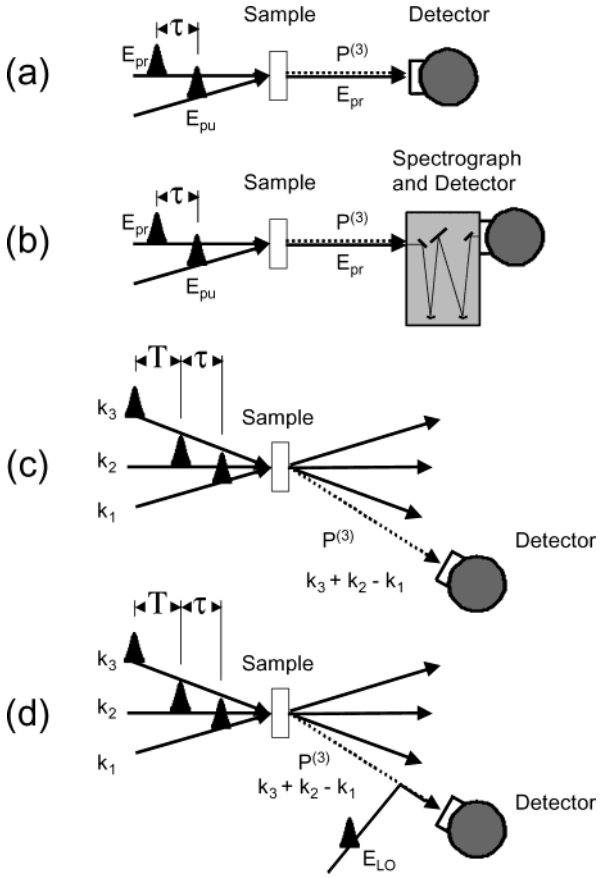

Figure 11. Experimental configurations for nonlinear infrared spectroscopy: (a) spectrally integrated pump−probe; (b) spectrally resolved pump−probe; (c) homodyne (intensity)-detected three-pulse photon echo; and (d) heterodyne (amplitude)-detected three-pulse photon echo.

$$\Delta\alpha(\omega_{pr}) = -\log\left[\frac{T(\omega_{pr})}{T_0(\omega_{pr})}\right] = \frac{4\pi\omega_{pr}}{cn(\omega_{pr})}\,\mathrm{Im}\int_{-\infty}^{\infty} \mathrm{d}t\; E_{pr}^{*}(t)P^{(3)}(t)/\int_{-\infty}^{\infty} \mathrm{d}t\;|E_{pr}(t)|^2 \quad (8)$$

Here, $T(\omega_{pr})$ and $T_0(\omega_{pr})$ represent the transmission of the sample with and without excitation, c is the velocity of light, $n(\omega_{pr})$ is the refractive index of the sample, and $E_{pr}(t)$ and $P^{(3)}(t)$ are the time-dependent electric field of the probe pulse and the third-order polarization in the sample, respectively. The third-order polarization contains the nonlinear response of the sample induced by the pump pulse and is theoretically described by, e.g., the formalism given in section 3.2. For a spectrally resolved detection of the probe pulse, the measured signal is given by

$$\Delta\alpha(\omega) = \frac{4\pi\omega_{pr}}{cn(\omega)}\,\frac{|E_{pr}(\omega)|^2\;\mathrm{Im}(P^{(3)}(\omega)/E_{pr}^{*}(\omega))}{\int_0^{\infty} \mathrm{d}\omega\;|E_{pr}(\omega)|^2} \quad (9)$$

Here, $E_{pr}(\omega) = \int_{-\infty}^{\infty} \mathrm{d}t\;\exp(i\omega t)E_{pr}(t)$ is the Fourier transform of the time-dependent probe field, and $P^{(3)}(\omega)$ is the nonlinear polarization component at the frequency ω.

Two-dimensional pump−probe spectroscopy of infrared-active vibrations represents a recently developed method which provides insight into couplings between different vibrational oscillators.[56,101] One of the oscillators is excited by a subpicosecond pulse of a bandwidth comparable to the vibrational line width, and the frequency-resolved transmission change is probed over the full spectral range in which the vibrational transitions of the different oscillators occur. The pump−probe signal consists of a transmission change originating from the oscillator excited by the pump and, more importantly, from oscillators which are not resonant with the pump but coupled to the oscillator excited. Such "off-diagonal" signals, which are observed on the $v = 0 \rightarrow 1$ and $v = 1 \rightarrow 2$ transitions of the coupled oscillator, are a measure of the microscopic coupling strength. Information on the orientation of the different transition dipoles can be derived from polarization-resolved measurements. The couplings between different oscillators give information on the underlying molecular structure, e.g., the arrangement of the coupled functional groups. This has been demonstrated for a number of biologically relevant systems such as small peptides.[102]

Femtosecond four-wave mixing techniques allow for a direct measurement of the macroscopic nonlinear polarization dynamics.[103,104] Recently, two- and three-pulse photon-echo methods have been applied to study the coherent response of resonant vibrational excitations in hydrogen bonds, in particular coherent O−H stretching excitations.[67,105−107] In general, vibrational photon-echo spectroscopy is based on the resonant interaction of three femtosecond pulses of a center frequency ω and propagation directions $\boldsymbol{k}_1$, $\boldsymbol{k}_2$, and $\boldsymbol{k}_3$ with the vibrational transition under study (Figure 11c,d). There is a time delay τ, the so-called coherence time, between pulses 1 and 2, and a delay T, the population time, between pulses 2 and 3. Thus, photon-echo spectroscopy is intrinsically multidimensional in the time domain. Interference of pulse 2 with the polarization generated by pulse 1 in the sample generates a transient frequency grating from which pulse 3 is scattered into the phase-matched directions $-\boldsymbol{k}_1 + \boldsymbol{k}_2 + \boldsymbol{k}_3$ and $+\boldsymbol{k}_1 - \boldsymbol{k}_2 + \boldsymbol{k}_3$. The diffracted signal is either homodyne-detected in a time-integrated way or heterodyne-detected by convoluting it with the field from a fourth phase-locked pulse which serves as a local oscillator. For an optically thin sample, small diffraction efficiency, and perfect phase-matching, the slowly varying amplitude approximation gives the following expression for the homodyne-detected intensity I_{HOM}:

$$I_{\mathrm{HOM}} = \frac{\pi\omega^2}{2n(\omega)c} l^2 \int_{-\infty}^{\infty} \mathrm{d}t \, |P^{(3)}(t,\tau,T)|^2 \qquad (10)$$

Here, l represents the interaction length in the sample and $P^{(3)}(t)$ the third-order polarization depending on the time delays τ and T. For heterodyne detection with a local oscillator of identical frequency ω, the signal I_{HET} is given by

$$I_{\mathrm{HET}} = \frac{n(\omega)c}{4\pi} \int_{-\infty}^{\infty} \mathrm{Re}[E_{\mathrm{LO}}^*(t)E_{\mathrm{s}}(t)]$$
$$\propto -(\omega l) \int_{-\infty}^{\infty} \mathrm{d}t \, \mathrm{Im}[E_{\mathrm{LO}}^*(t)P^{(3)}(t,\tau,T)] \qquad (11)$$

where $E_{\mathrm{LO}}(t)$ and $E_{\mathrm{s}}(t)$ are the electric field originating from the local oscillator and the nonlinear polarization, respectively.[55]

Different types of four-wave-mixing measurements bring out different aspects of the ultrafast vibrational dynamics, depending on the particular choice of the two time delays τ, the coherence time, and T, the population time:

(i) Transient grating scattering, in which pulses 1 and 2 of zero mutual delay ($\tau = 0$) generate a population grating, and the signal diffracted from this grating is measured as a function of the population time T. The measured signal decay gives insight into population relaxation, i.e., the lifetime of the excited vibrational states, and/or other relaxation processes affecting the grating amplitude, e.g., rotational diffusion.

(ii) In a two-pulse photon echo (2PE), the population time is set to zero ($T = 0$); i.e., the second and third pulses interact with the sample simultaneously. The signal is measured as a function of the coherence time τ and gives insight into the overall decay of the macroscopic coherent polarization in the sample. For a homogeneously broadened ensemble of oscillators, the coherent response follows a free-induction decay. The homodyne-detected two-pulse photon-echo signal peaks at $\tau = 0$ and decays with $T_2/2$ (T_2 is the dephasing time). In contrast, inhomogeneous broadening results in a photon-echo-like behavior, i.e., a finite shift τ_{max} of the maximum signal to positive τ values and a decay with $T_2/4$.

(iii) In a three-pulse photon echo (3PE), both time delays τ and T are varied in order to monitor the polarization dynamics in a more complete way. Three-pulse photon echoes allow for a distinction of different dephasing processes and the underlying couplings.[108]

(iv) In a three-pulse echo peak shift measurement (3PEPS), one determines for each value of T the coherence time $\tau_{\mathrm{max}}(T)$ at which the photon-echo signal is maximum. The decrease of $\tau_{\mathrm{max}}(T)$ with T indicates the decrease of inhomogeneity in the optical response by spectral diffusion processes. It has been shown for two-level systems that the echo peak shift mimics the frequency fluctuation correlation function for time delays T at which the temporal overlap of the three optical pulses is negligible.[109,110]

5. Coherent Response of O–H/O–D Stretching Vibrations

In this section, recent results in infrared photon-echo[67,105,107,111,112] and transient hole-burning spectroscopy[113−122] are discussed that have revealed much information on the coherence properties of O−H/O−D stretching vibrations. We first describe experiments on the important system of HOD in D_2O in section 5.1. HOD in D_2O is expected to show ultrafast structural dynamics of hydrogen bonds, similar to

water. The dephasing of coherent O−H/O−D stretching excitations by the fluctuating force of the environment should reflect such structural fluctuations. On the other hand, population relaxation of O−H/O−D stretching excitations in HOD in D_2O should be different from those of water because of the different vibrational level schemes and couplings. In the following, we address both the coherence decay of the O−H/O−D stretching vibration as probed by two-pulse photon-echo spectroscopy and spectral diffusion of the O−H/O−D stretching transition studied in three-pulse photon-echo and hole-burning spectroscopy. This discussion of experimental results is complemented by recent theoretical studies that aim to connect the experimental findings to microscopic mechanisms.[27,28,45,46,123,124] Results on the coherent evolution of low-frequency wave packet motions which are observed in medium-strong hydrogen bonds with ultrafast infrared pump−probe spectroscopy are presented in section 5.2.[112,125−128] Next we turn to recent photon-echo studies of molecular systems with medium-strong hydrogen bonds,[106,112,129] demonstrating the relevance of the multilevel structure of the vibrational transition for understanding the observed signals.

5.1. Dephasing and Spectral Diffusion of the O–H Stretching Vibration of HOD in D_2O

5.1.1. Dephasing of the O–H Stretching Vibration of HOD in D_2O

Photon-echo spectroscopy has been the standard technique to elucidate the homogeneous and inhomogeneous contributions to the absorption line shape for decades. The two-pulse photon-echo sequence determines the coherence decay after the first field interaction (coherence time t_1, cf. Figure 1), where the second evolution period is set to zero (population period $t_2 = 0$). Any phase memory not disturbed by the fluctuating environment rephases during the third period (coherence time t_3). A macroscopic photon echo is then detected as a function of the delay time τ between the two pulses, directly probing the coherence loss of the system (we refer to Figure 9 for the Liouville space pathways). The first picosecond infrared photon echo, using a free electron laser, obtained on a metallocarbonyl compound, was reported in 1993 by Zimdars et al.[130] It took several years of laser development until the first femtosecond infrared photon echo on a hydrogen-bonded O−H stretching mode, of HOD in D_2O, was detected with a tabletop laser system.[105] In the latter study of Stenger et al., where 130 fs pulses and homodyne detection of the diffracted signal were used, an extremely rapid coherence decay of 33 fs was observed for the O−H stretching mode, independent of the excitation frequency (Figure 12). In the simplest approach, based on a Bloch model, the data were described by a homogeneous line-broadening mechanism with a dephasing time of 90 fs, contributing about half of the total line width of the O−H stretching band. On the time scale of the two-pulse photon-echo experiment, the remaining part of the line broadening was treated as being inhomogeneous. As discussed in ref 105, a more sophisticated modeling by a transition frequency correlation function with (a) a Gauss−Markov modulation process with a correlation time of 30 fs and (b) a spectral diffusion process with a time constant of 700 fs gave fitting results reproducing the data equally well. Experiments with an improved pulse duration of 70 fs and heterodyne detection, reported by Yeremenko et al., confirmed the extremely fast decay of vibrational coherence and led to a similar bimodal fitting with time constants of 130 and 900 fs.[107]

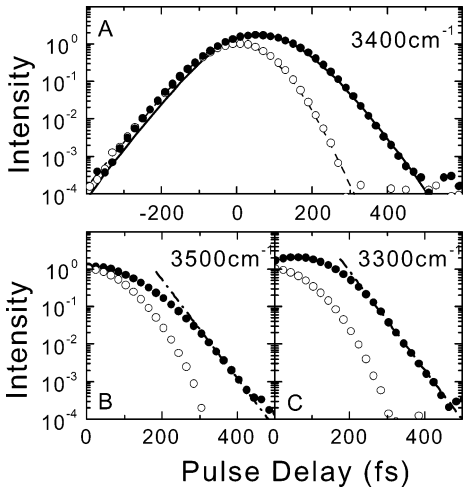

Figure 12. Integrated two-pulse photon-echo signal as a function of pulse delay time recorded at three spectral positions in the O−H stretching band of HOD:D_2O, represented as solid dots. The open circles indicate the time resolution as determined with a CaF_2 sample. The solid line is a global fit of the water data, and the dashed line is a fit of the instantaneous response. All curves show an intensity echo signal decay with a slope of 33 fs (dash−dotted line). Reproduced with permission from ref 105. Copyright 2001 American Physical Society.

The extremely fast dephasing of the O−H stretching excitation represents a major difference from the stretching vibrations of free O−H groups. The dephasing time of stretching excitations of free O−H/O−D groups has not been the subject of photon-echo studies yet. Assuming a predominant homogeneous broadening, one estimates a lower limit for the dephasing time of about 1 ps from the line width of 10 cm^{-1}. In ref 105, the much faster dephasing in hydrogen bonds was rationalized by using the vibrational dephasing theory pioneered by Oxtoby.[57] Developing the interaction potential between the O−H oscillator and the surrounding solvent in powers of the vibrational coordinate q of the O−H stretching oscillator, one derives for the fluctuating transition frequency shift $\delta\omega(t)$

$$\hbar\delta\omega(t) = (q_{11} - q_{00})F_1(t) + [(q^2)_{11} - (q^2)_{00}]F_2(t) + \ldots \quad (12)$$

where q_{ii} and $(q^2)_{ii}$ ($i = 0, 1$) are matrix elements to be taken in the $v_{OH} = 0, 1$ states, and $F_{1,2}(t)$ are the fluctuating forces of the solvent. The first term, describing the influence of the linear force exerted by the solvent, disappears for a harmonic oscillator with $(q_{11} - q_{00}) = 0$; i.e., the energy levels of a harmonic oscillator are modulated in the same way by the linear force, resulting in a constant $v = 0 \rightarrow 1$

transition frequency. In contrast, the transition frequency in an anharmonic oscillator is affected by $F_1(t)$. It has been shown for two very different anharmonic systems, weakly interacting liquid N_2[57] and strongly interacting CN^- in water,[131] that this term dominates dephasing indeed. In this limit, the (pure) dephasing rate $1/T_2^*$ is proportional to the product of the anharmonicity Δ of the vibration and the time integral of the correlation function of the linear force exerted by the solvent:

$$(1/T_2^*) \propto \frac{|\Delta|}{\hbar^2\omega^2\mu} \int_0^\infty \langle F_1(t)F_1(0)\rangle \, dt \qquad (13)$$

where ω and μ are the vibrational frequency and dipole moment, respectively. Comparing the anharmonic shifts of non-hydrogen-bonded O−H stretching modes of $\Delta \leq 100$ cm^{-1} [132] with that of hydrogen-bonded O−H vibrations ($\Delta = 270$ cm^{-1} [133]), such numbers account in a semiquantitative way for the much higher dephasing rates in hydrogen-bonded systems. In a microscopic picture of solute−solvent coupling, the increase of the O−H stretching anharmonicity as a consequence of hydrogen bonding makes the oscillator attackable by the fluctuating force $F_1(t)$ and gives rise to extremely fast dephasing. It should be noted that similar conclusions have been reached by Piryatinski et al.[123]

5.1.2. Spectral Diffusion of the O–H Stretching Vibration of HOD in D_2O

Determination of the full transition frequency fluctuation correlation function, $C(t)$, is necessary for understanding the structural fluctuations of the hydrogen-bonded network. Experimental approaches to elucidate $C(t)$ are three-pulse photon-echo and transient hole-burning spectroscopy. In particular, both techniques are sensitive to spectral diffusion, the process of diminishing the inhomogeneous distribution existing at time $t = 0$ by solvent motions. Any persistence of $C(t)$ for longer times thus indicates structural correlation of the liquid at the same times. When one pumps an inhomogeneously broadened transition with a laser pulse whose bandwidth is smaller than the spectral width of that transition, only a fraction of the molecular ensemble is promoted to the first excited state (Figure 13). Here, a population distribution in the excited state is created (particle) that mirrors the hole left in the ground-state population distribution. In pump−probe spectroscopy, the interactions with the laser field occur in such a way that no evolution occurs during the first coherence time period, $t_1 = 0$ (Figure 9). For systems with an excited state and a ground state displaced along the solvation coordinate representing the solute−solvent interaction, the particle and hole will subsequently move to their respective energetic minima when the surrounding solvent reacts to the nonequilibrium population distributions during the population period, t_2. The sign of the displacement determines the direction in which these particle and hole relaxations will occur. This effect is known as the dynamic Stokes shift and has been observed and analyzed for electronic transitions (Figure 13a). If,

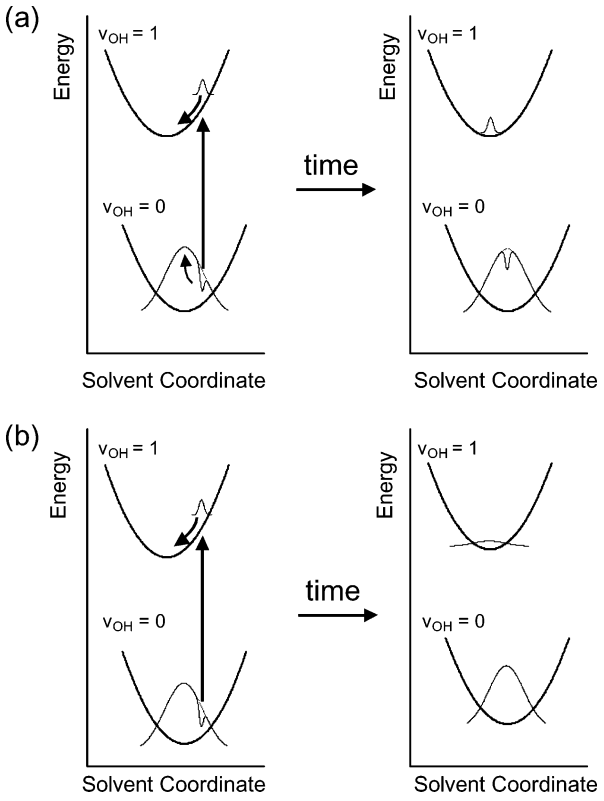

Figure 13. Two prototypical cases that may occur in a transient hole-burning experiment. A fraction of the inhomogeneous distribution along a solvent coordinate is promoted to the $v_{OH} = 1$ excited state at the frequency of the applied laser pulse, forming a particle in $v_{OH} = 1$ and leaving a hole in the $v_{OH} = 0$ ground-state distribution. In (a), the particle adapts to the new equilibrium configuration over the course of time due to solvent rearrangement, in a fashion similar to that by which the hole rearranges. In (b), the particle and hole eventually wash out due to solvent fluctuations.

on the other hand, the noninstantaneous population distributions are washed out due to the fluctuating solvent environment, spectral diffusion occurs, meaning that a certain subset of solute−solvent configurations are eventually randomly distributed over all possible situations (Figure 13b). An experimental configuration that directly probes the time evolution of the nonstationary particle and hole distributions is transient hole-burning, where a broadband probe pulse monitors the transient absorbance changes after narrow-band excitation of the pump pulse; i.e., the nonlinear polarization is self-heterodyne-detected during coherence period t_3.

Gale et al.[117−119] and Woutersen et al.[120] have measured transient pump−probe spectra using independently tunable 150−200 fs pump and probe pulses (65−70 cm^{-1} bandwidth). Gale et al., using a band moment analysis, observed a shifting of the transient absorbance change toward the center of the O−H stretching band with a time constant of 700 fs, regardless of where the pump frequency is tuned. Woutersen et al. observed a more delayed rise when pump and probe tuning frequencies were farther apart. A time constant of 500 fs for a vibrational dynamic Stokes shift was deduced from this study. In a more recent combined effort of the Bakker and Gale groups, pump−probe results clearly show how

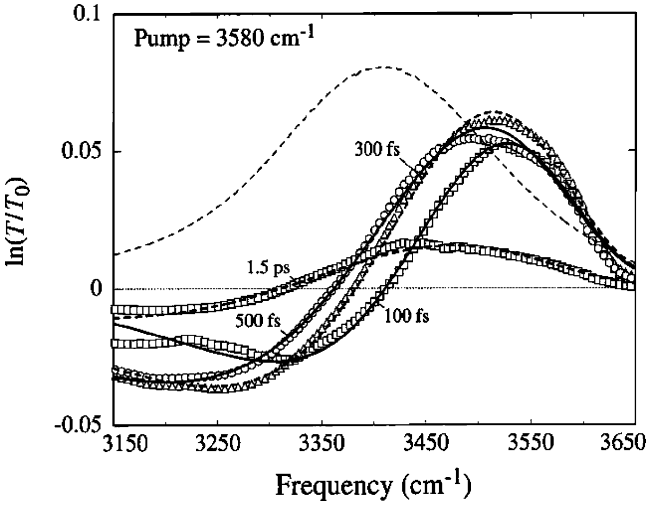

Figure 14. Transient spectra of 0.5 M HOD dissolved in D_2O in a hole-burning experiment measured at four pulse delays after pump excitation at 3580 cm^{-1}. The solid curves represent calculated spectra obtained with a modified quantum-mechanical Lippincott−Schroeder model. The dashed curve is the experimental linear absorption spectrum of the O−H stretching vibration of HOD:D_2O. Reproduced with permission from ref 122. Copyright 2002 American Institute of Physics.

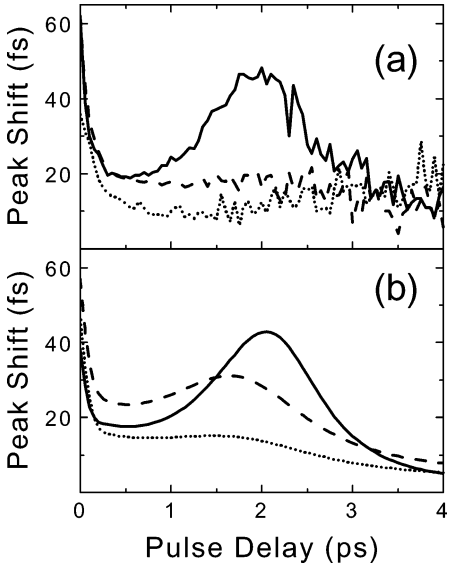

Figure 15. (a) Experimental three-pulse photon-echo peak shift data for laser pulses centered at 3300 (solid line), 3400 (dashed line), and 3500 cm^{-1} (dotted line). (b) The calculated signals, where the correlation function was assumed to consist of three components governed by a homogeneous dephasing, $T_2 = 90$ fs, and two Kubo terms with correlation times of 700 fs and 15 ps (adapted from ref 67).

the red-shift of the hole, when pumping at the high-frequency side of the O−H stretching band, is accompanied by a broadening[122] (Figure 14). The latter fact, together with the previous observations, demonstrates that spectral diffusion is the dominating mechanism (above a mere Stokes shift in one direction) that occurs on a subpicosecond time scale. The different line shapes of the $v_{OH} = 0 \rightarrow 1$ and the $v_{OH} = 1 \rightarrow 2$ transitions derived from hole and particle contributions to the transient absorbance changes have been analyzed with a refined Lippincott−Schroeder model for the vibrational system where the O−H stretching and O−H···O hydrogen bond modes are coupled. A spectral diffusion time constant of 950 ± 100 fs was derived for the O−H stretching mode in both $v_{OH} = 0$ and $v_{OH} = 1$ states, with an additional fast component of 170 ± 40 fs in the excited $v_{OH} = 1$ state, ascribed to hydrogen bond contraction after O−H stretching excitation.

Different observations have been made in studies by Laenen et al.[113−116] This is likely due to the somewhat larger pulse durations applied. The use of 1 ps pulses of smaller bandwidth aimed at analyzing the spectral substructure of the O−H stretching band of HOD:D_2O; i.e., does this band consist of several sub-bands, each representing a different hydrogen-bonding structure? Laenen et al. claim the existence of three distinct hydrogen-bonded water structures:[113,114] an ice-like tetrahedral geometry, a partially hydrogen-bonded species (both with a spectral line width of 60−80 cm^{-1}), and an even more loosely bound form (with a spectral width of 140 cm^{-1}). In later reports,[115,116] four spectral components were ascribed to either local tetrahedral ice-like or more weakly bound hydrogen-bonded structures, and to two combination bands in the O−H stretching spectral region. In light of the results of the two-pulse photon-echo study by Stenger et al.,[105] suggesting a homogeneous line width of about 120 cm^{-1}, and transient hole-burning results by the Gale and Bakker groups, showing a substantial spectral diffusion on subpicosecond time scales, the conclusions of Laenen et al. are likely due to overinterpretation. Apart from the problem of coherent coupling effects between pump and probe pulses (due to diagrams V−X in Figure 9)[134] that erroneously may suggest dynamics at early delay times, it remains hard to substantiate experimental evidence of distinct structural features at delay times longer than 1 ps. We come back to this problem in the next subsection when discussing recent numerical studies. On the other hand, HOD:D_2O is not fully relaxed on a time scale of 1−2 ps, as is indicated by recent three-pulse echo experiments on HOD:D_2O.[67]

From Figure 12, it is clear that the two-pulse photon echo has its maximum at positive delay times (+45 fs). Such an echo peak shift is indicative of inhomogeneity in the transition. The two-pulse photon echo is a limiting case of the three-pulse photon echo with the second time period, t_2, where population terms evolve in time, equal to zero. When probing the maximum of the three-pulse photon-echo signal as a function of the coherence time t_1 for different population periods t_2, a decay of the echo peak shift (3PEPS) reflects a decay of the inhomogeneity due to spectral diffusion. From previous work on electronic transitions of dye molecules in solution, it has been shown that the 3PEPS decay directly reflects the time behavior of $C(t)$.[109,110] This technique was also demonstrated in the infrared in experiments on the azide ion in water.[135] In Figure 15, we show the 3PEPS signals obtained at three distinct spectral positions in the O−H stretching band of HOD:D_2O.[67] After a rapid decay for all three spectral positions within the time resolution of the experiment, the 3PEPS signal decays further on the high-frequency

end and at the center of the band. On the low-frequency part of the band, however, the 3PEPS signal appears to increase again, reaching a maximum around a delay time of 2 ps, after which it decays again. The experimental results, which clearly do not mimic a continuously decaying $C(t)$, can be explained by taking into account the five-level structure of hydrogen-bonded O−H stretching vibrations (Figure 8). In the extensive survey by Stenger et al.,[67] several cases have been inspected where the influence of long-tail components in $C(t)$ and phase memory conservation vs phase memory loss upon T_1 relaxation from $v_{OH} = 1 \rightarrow 0'$ have been looked at. It is clear from this analysis that the observed 3PEPS signals (within the frame of Kubo's stochastic modulation model) point to a $C(t)$ with temporal components at sub-100 fs, 700 fs, and 5−15 ps, together with a loss of phase memory upon T_1 relaxation from $v_{OH} = 1 \rightarrow 0'$. The relaxation channel shown schematically in Figure 8 combines a complex sequence of relaxation steps (see also section 6), including transient population of the O−H and O−D bending modes,[136] equilibration of the vibrational system,[137] and thermal diffusion. This crude simplification is justified by (i) the fast time scale of the whole sequence of processes and (ii) the fact that the photon echo giving rise to the peak shift behavior originates from the original bleach, and not the transient products.

A recent photon-echo study with improved time resolution[111] has revealed an underdamped oscillatory contribution to the 3PEPS signal, ascribed to motions of the hydrogen bond mode. This small, underdamped oscillatory component has been predicted by molecular dynamics simulations.[27,28,46,123,124]

In summary, photon-echo and transient hole-burning spectroscopy on the O−H stretching vibration of HOD:D_2O suggest that $C(t)$ decays on three distinct time scales, with time constants of ≤100 fs, 700−950 fs, and 5−15 ps. The main result of all experiments is that memory on the O−H stretching frequency is preserved for extended times, hinting at relatively long-lived structural correlations of the hydrogen bonds in liquid water. In this context, we note that polarization-sensitive infrared pump−probe spectroscopy has revealed a rather slow polarization anisotropy decay of the O−H stretching transition of HOD:D_2O that occurs with time constants $\tau_{rot} = 2.6$ ps ($v_{OH} = 0$) and $\tau_{rot} = 4.2$ ps ($v_{OH} = 1$) at 298 K.[138−141] Clearly, the hydrogen-bonding networks in water inhibit free rotation, and thus randomization, of liquid structure on these time scales. The question of how to interpret this finding in more microscopic detail is treated in the following section.

5.1.3. Theoretical Studies on Dephasing and Spectral Diffusion of HOD in D_2O

The femtosecond infrared experiments on HOD:D_2O give direct access to the temporal behavior of the transition frequency correlation function $C(t)$. A central question consists of linking the correlation function $C(t)$ to structural relaxation of water on a microscopic molecular level. As indicated in section 2.1, the transition frequency of the O−H stretching vibration is correlated to the hydrogen bond distance and thus is connected to hydrogen bond strength, as deduced empirically from a large range of hydrogen-bonded systems in the solid-state.[12,13,26] In a standard interpretation of the femtosecond infrared experiments described above, this correlation between O−H stretching frequency and hydrogen bond length is used for a single molecular species in the liquid state. In this case, the more red-shifted an O−H stretching vibration in a particular HOD molecule absorbs, the more strongly this molecule is hydrogen-bonded through its O−H group to neighboring water molecules. The decay of $C(t)$ is then interpreted as a decay of correlation in hydrogen bond distance (and in hydrogen bond strength). Two different reasons for this decay are commonly proposed: either $C(t)$ indicates the time scale of fluctuations of hydrogen bond lengths[105,117−119,122] or it gives access to the hydrogen bond reorganization time scale due to a continuous process of breaking and formation.[67,107,113,114] Earlier molecular dynamics simulations[142−149] dealt with the calculation of average hydrogen bond lifetimes for pairs of hydrogen-bonded molecules and how structural networks are reorganized. Since these average hydrogen bond lifetimes appear to have values similar to those found for the characteristic decay constants for $C(t)$, hydrogen bond breaking and formation is often assumed to play a major[113,114] but sometimes not the only[67,107] role in the dynamics.

Such concepts have been critically assessed in recent theoretical studies.[27,28,45,46,54,123,124] Diraison et al. have studied the D_2O liquid solvent response to vibrational excitation of the solute H_2O[54] using a mixed quantum−classical method, with the intramolecular degrees of freedom of H_2O treated quantum mechanically and the rotational−translational degrees of freedom as well as the solvent computed by classical molecular dynamics simulation. The response functions of the three vibrational normal modes of H_2O (asymmetric stretching, symmetric stretching, and bending vibrations) all show a bimodal behavior with about equal magnitudes and with time constants of 50 and 800 fs, ascribed to rearrangements in the hydrogen bond network after vibrational excitation. In this study, hydrogen bond breaking and formation was not included.

In a more advanced modeling by Rey, Møller, and Hynes[27] and Lawrence and Skinner,[28,45,46,123,124,150] different aspects of microscopic dynamics have been addressed, in particular the validity of the presumed one-to-one correlation between the O−H stretching frequency v_{OH} and the OH···O hydrogen bond length R_{O-O}. Both groups have found a large dispersion in R_{O-O} for a given value of v_{OH} in the case of HOD:D_2O, much larger than the already scattered data obtained on the series of hydrogen-bonded solids. Figure 3 shows the resulting correlation calculated by the Skinner group[28,150] (a similar behavior has been reported by the Hynes group[27]). For HOD:D_2O, a substantial dispersion has also been found in the correlation between O−H stretching frequency v_{OH} and the OH···O hydrogen bond bending angle α_{OH-O}, defined as the angle between the O−H bond and the

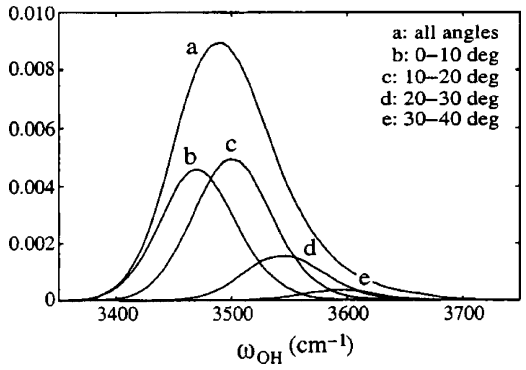

Figure 16. Probability distribution of the O−H stretching frequency for HOD:D_2O pairs with the O···O distance $R = 0.28 \pm 0.01$ nm and its separation into different bending angles α at intervals (taken from ref 27).

O···O bond vectors (Figure 16). Lawrence and Skinner argue that, due to the much weaker correlation, it is less meaningful to interpret frequency fluctuations as being due to angular motions.[150] In contrast Rey, Møller, and Hynes deduce from this finding that the latter dispersion actually makes the interpretation of the O−H stretching frequency ν_{OH} as a one-to-one corresponding structural probe the most problematic.[27]

$C(t)$ is found by both groups to decay first on a sub-100 fs time scale (time constants given by Rey et al. as 66 fs on the high-frequency side and 31 fs on the low-frequency side of the O−H stretching band and as 40 fs by Lawrence and Skinner), followed by a weak recurrence at 140−170 fs (corresponding to a frequency of 200−240 cm^{-1}), and a subpicosecond component (time constants given by Rey et al. as 863 fs on the high-frequency side and 496 fs on the low-frequency side and as 500 fs by Lawrence and Skinner). Whereas Rey et al. ascribe the fast component with the recurrence to underdamped motion of the low-frequency O−H···O stretching mode, Lawrence and Skinner give hydrogen bond length fluctuations as the main reason for this initial fast decay. These authors have also reproduced the vibrational line shape and spectral shift, where they have explored the Gaussian nature of the frequency fluctuations[46] and have critically assessed the modeling of the two- and three-pulse photon echo by use of Kubo's stochastic modulaton model.[123,124] Both the Hynes and Skinner groups have analyzed the subpicosecond component to be due to hydrogen bond breaking and (re-)formation dynamics. When regarding water as consisting of different species with different instantaneous degrees of hydrogen bonding, Lawrence and Skinner have decomposed the O−H stretching band into four components, where a particular HOD molecules is part of either four, three, or two hydrogen bonds.[150] Although this is reminiscent of the ansatz of Laenen et al.,[113−116] we note here that structural fluctuations and breaking and formation of hydrogen bonds occur definitely on subpicosecond time scales, in such a way that exchanges between these structures are expected to take place on the same time scale. On the other hand, the photon-echo peak shift study by Stenger et al.[67] has shown an extended tail in $C(t)$ decaying with a time constant of 5−15 ps, from which we conclude that if hydrogen bonds are broken on a subpicosecond time scale, these bonds have a finite probability to re-form to similar structural features as before they are broken, only to lose correlation completely after a large number of hydrogen bond breaking/re-formation cycles. Until now, molecular dynamics studies have been performed only to delay times of 1−1.5 ps. In addition, the five-level scheme of Figure 8 has not been implemented so far, and so the slower picosecond dynamics needs further theoretical consideration.

5.2. Wave Packet Motions of Low-Frequency Modes in Medium-Strong Hydrogen Bonds

In this section we discuss recent ultrafast infrared pump−probe measurements on intra- and intermolecular medium-strong hydrogen bonds where wave packet motions of low-frequency hydrogen bond modes have been demonstrated after coherent excitation of the O−H stretching bands.[112,125−128] Coherent motion of vibrational wave packets of low-frequency modes have been observed in numerous studies on vibronic transitions. Impulsive stimulated Raman scattering with excitation off-resonant with respect to the electronic transitions leads to the coherent preparation of wave packets in the electronic ground state.[151] Excitation resonant with electronic transitions leads to the coherent preparation of wave packets both in the electronic ground and excited states,[100] where the efficiency of the latter process is usually larger for the case of long electronic excited-state lifetimes.[152−154] When the excited-state lifetime is short compared to the coherence decay times of the wave packet motions, the ground-state contributions to the observed signals become more dominant. In addition, vibrational coherent wave packet motion has also been observed for cases where the coherence is driven by rapid nonradiative processes, where wave packets are observed in product states.[155−158] For electronic two-level systems, inspection of the amplitude and phase of the oscillatory pump−probe signals due to wave packet motions[159] has shown that, in the case of off-resonant impulsive stimulated Raman scattering, a 180° phase jump occurs at the center frequency of the excitation pulse. The initial phase for the off-resonant, impulsively driven, ground-state wave packet is 90°. In contrast, for the case of resonantly enhanced coherent low-frequency mode excitation, the phase jump of 180° occurs at the maximum of the absorption band. By scanning over the whole absorption band, a total phase change of 360° occurs, whereas the phase flip for the excited-state wave packet near the emission maximum is 180°. The excited-state wave packet has a phase of either 0 or 180°, whereas the phase of the resonantly driven ground-state wave packet depends on the detuning of the excitation and detection frequencies relative to the 0−0 transition, and on the displacement sign of the potential energy surfaces, resulting in varying values between 0 and 360°.

It is very important to investigate whether in the case of hydrogen-bonded O−H/O−D stretching modes, where similar potential energy surfaces for low-frequency modes have been defined as for vibronic systems (see section 2), coherent wave packet motions

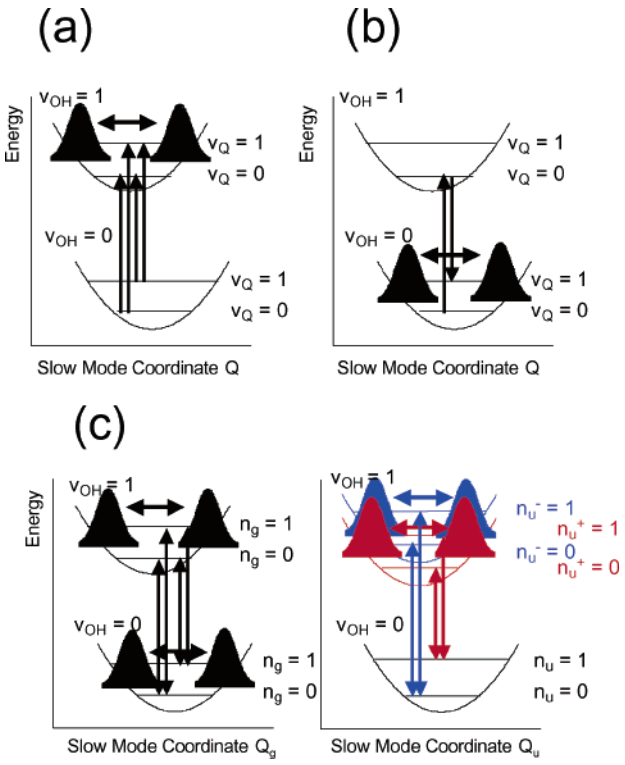

Figure 17. Schematic representation of the wave packet generation upon coherent excitation of the O−H/O−D stretching modes in hydrogen bonds, showing the excited-state wave packet (a) and the ground-state wave packet (b) in a single hydrogen bond. Due to Davydov coupling and transition dipole selection rules in cyclic acetic acid dimer, no wave packet between n_u^- and n_u^+ states can be generated. In panel (c), only wave packets in either of these states of the Q_u mode can occur, whereas the Q_g mode shows the standard behavior for wave packet generation.

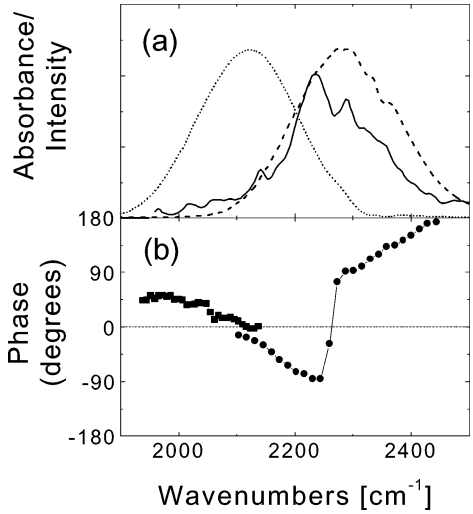

Figure 18. (a) Stationary absorption spectrum of HBT-D in toluene with spectra of excitation pulses centered at 2120 (dotted line) and at 2300 cm^{-1} (dashed line). (b) Phase of the oscillatory contributions for the red (squares) and blue (dots) excitation pulses. A phase jump by 180° occurs at the center of the absorption band, independent of the excitation pulse. Reproduced with permission from ref 126. Copyright 2001 Elsevier Science.

can also be generated (Figure 17). The observation of such wave packets would represent an independent time-domain confirmation of the anharmonic coupling between the hydrogen stretching mode and low-frequency hydrogen bond modes. Moreover, the coherent time-domain response of the coupled system sheds new light on the highly controversial issue of to what extent the low-frequency motions are over- or underdamped. Since the Franck−Condon progressions are more pronounced the larger the displacement of the potential energy surfaces is, i.e., the larger the anharmonic coupling between O−H/O−D stretching and hydrogen bond modes, medium-strong hydrogen bonds represent interesting test cases to explore such phenomena.

Recently, underdamped low-frequency wave packet motions have been observed along moderately strong intramolecular hydrogen bonds with well-defined geometries, namely in phthalic acid monomethyl ester (PMME-H),[127] its deuterated analogue (PMME-D),[125] and the deuterated analogue of 2-(2′-hydroxyphenyl)benzothiazole (HBT-D).[126] The wave packet motions have been detected in femtosecond infrared pump−probe spectroscopy as coherent modulations of the pump−probe signals on the O−H/O−D stretching transition, where the probe transmission was detected either spectrally integrated[127] or after spectral dispersion using a monochromator and detector array.[112,125,126,128] The wave packet motions have a dephasing time on the order of 1−2 ps. In all cases, oscillatory contributions due to a single coherently excited low-frequency mode have been detected. Comparison of the observed frequencies of these oscillatory pump−probe signals with standard far-infrared and Raman spectra and a vibrational analysis of these molecular systems by quantum chemical calculations have shown that the coherent wave packet motions are due to a 100 cm^{-1} out-of-plane hydrogen bond deformation mode (PMME-H/PMME-D) or a 120 cm^{-1} in-plane hydrogen bond deformation mode (HBT-D). Whenever a particular low-frequency vibration exhibits a large modulation of the hydrogen bond distance, the anharmonic coupling with the O−H/O−D stretching vibration is also substantial, and thus a major contribution to the coherent modulations in pump−probe spectroscopy occurs. Due to the short lifetime of the $v_{OH} = 1$ state, the wave packet generated via a resonantly enhanced Raman process in the $v_{OH} = 0$ state dominates the oscillatory pump−probe signal. For HBT-D, this behavior is evident from a phase jump of the oscillations by 180° at probe frequencies close to the center of the O−D stretching band (Figure 18). In the case of PMME-H/PMME-D, however, wave packet motions in the $v_{OH/OD} = 1$ state have been identified by probing on the $v_{OH/OD} = 1 \rightarrow 2$ transition (Figure 19). Quantum chemical calculations on PMME-H/PMME-D show that, besides the 100 cm^{-1} out-of-plane deformation mode, several other modes couple significantly to the O−H/O−D stretching mode.[127,160−164] These other modes, including the O···O hydrogen bond stretching mode and the O−H/O−D bending mode, have frequencies above 300 cm^{-1}, and thus a coherent excitation is not possible within the spectral bandwidth of 130 fs infrared pulses.

Acetic acid dimer, a prototype for medium-strong intermolecular hydrogen bonds, has only recently been studied with ultrafast infrared spectroscopy.

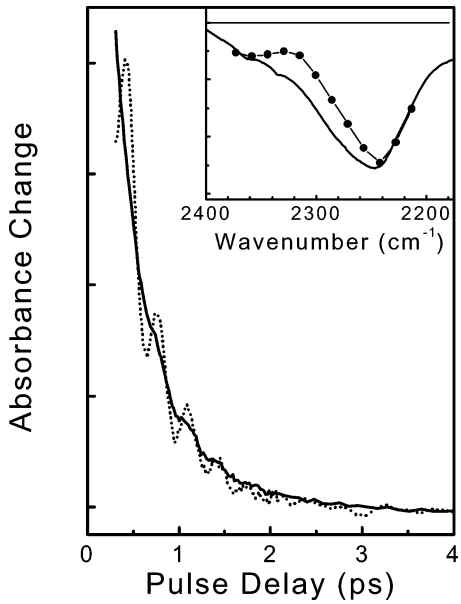

Figure 19. Decay of the excited-state $\nu_{OD} = 1 \rightarrow 2$ absorption of PMME-D showing an excited-state wave packet (dotted line) recorded at 2028 cm^{-1}. For comparison, the temporal behavior of the excited-state stimulated emission $\nu_{OD} = 1 \rightarrow 0$ frequency component obtained with a singular value decomposition procedure is shown as a solid line ($T_1 \simeq 400$ fs), together with the spectral representation in the inset (adapted from ref 125).

Such experiments have given insight into coupling between the two carbonyl groups in the dimer[49] and into vibrational relaxation processes.[165] Oscillatory contributions to pump−probe signals due to two hydrogen bond modes have very recently been observed in different isotopomers of the acetic acid dimer, $(CD_3COOH)_2$ (protonated dimer), $(CH_3COOD)_2$ (deuterated dimer), and $(CD_3COOH)-(CD_3COOD)$ (mixed dimer)[112,128,129] (Figure 20). Besides a weakly contributing 50 cm^{-1} mode, strongly coupled in-plane hydrogen bond deformation and stretching modes modulate the pump−probe signal with frequencies around 150 cm^{-1}. It should be noted that the coupling to more than one low-frequency mode represents a fact that is essential for a correct modeling of the linear O−H/O−D stretching absorption and has not been considered so far.

In the cyclic acetic acid dimer with two identical hydrogen bonds, i.e., the isotopomers $(CD_3COOH)_2$ and $(CH_3COOD)_2$, the resonant (Davydov) coupling of the oscillators leads to an energy splitting of the $\nu_{OH} = 1$ states. The dipole selection rules for this case have have been discussed in section 2.3, and result in two separate progressions of vibrational lines originating from the $n_{i,u} = 0$ and $n_{i,u} = 1$ levels in the $\nu_u = 0$ state (blue and red arrows in Figure 7). Since the macroscopic pump−probe signal is determined by the time evolution during the population period t_2, where the molecular systems are in population states given by the diagonal elements of the density matrix, only one sort of coherent superposition is possible in an individual molecule, depending on whether the $n_{i,u} = 0$ or $n_{i,u} = 1$ level is populated for a particular low-frequency mode i. The two resonantly (Davydov) split polarization components originate from different molecules, giving rise to independent additive contributions to the pump−probe signal (Figure 17c). As a result, there is no quantum beat between lines belonging to different progressions; i.e., oscillatory signals reflecting the resonant coupling V_0 are absent for a sequential interaction between pump and probe. This conclusion is supported experimentally by pump−probe signals of the mixed dimer $CD_3COOH-CD_3COOD$, where any resonant coupling of stretching oscillators is absent. Such signals display the same oscillatory features as those from the dimers with two identical hydrogen bonds. It should be noted that the ground-

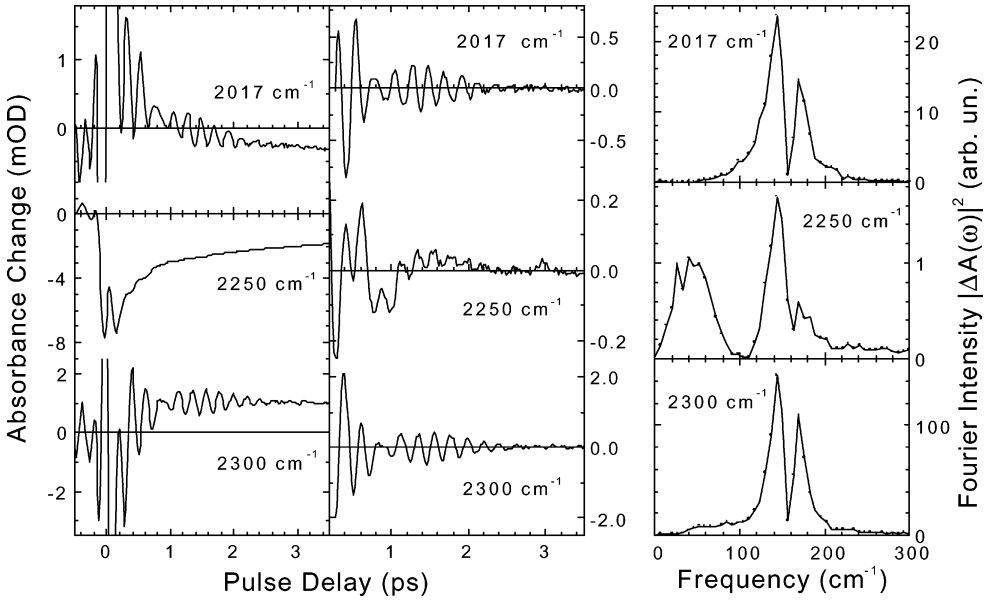

Figure 20. (Left) Pump−probe signals obtained on $(CH_3COOD)_2$ in CCl_4 for three detection frequencies. (Center) The oscillatory components (obtained after subtraction of the incoherent dynamics) showing a pronounced beating pattern. Fourier transformation of these traces indicates three frequency components, ascribed to a weakly contributing 50 cm^{-1} mode, and to strongly coupled hydrogen bond deformation and stretching modes around 150 cm^{-1}. Reproduced with permission from ref 128. Copyright 2003 Elsevier Science.

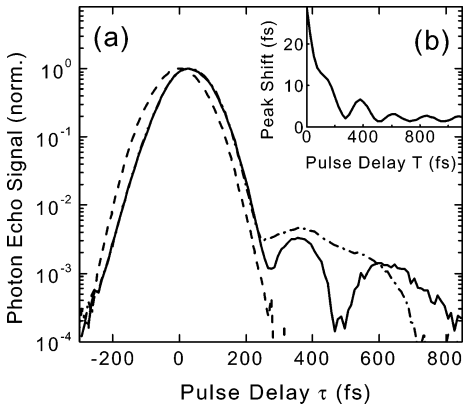

Figure 21. (a) Two-pulse photon-echo results obtained on the O−H stretching transition of the mixed $CD_3COOH-CD_3COOD$ (solid line) and pure $(CH_3COOH)_2$ (dash−dotted line) acetic acid dimers with femtosecond pulses centered at 2940 cm^{-1}. The temporal resolution is indicated by the instantaneous signal response obtained on the pure solvent CCl_4 (dashed line). (b) Three-pulse echo peak shift showing a rapid diminishing and oscillations due to a coherent excitation of the low-frequency modes. Reproduced with permission from ref 129. Copyright 2003 American Physical Society.

state wave packets are induced via a resonantly enhanced Raman process in the $Q_{i,g}$ modes.

5.3. Dephasing of O–H Stretching Vibrations in Medium-Strong Hydrogen Bonds

Molecular systems with medium-strong hydrogen bonds exhibit O−H/O−D stretching vibrational bands with extensive spectral broadening exceeding 500 cm^{-1}.[13,15,16] This also occurs for systems with a well-defined geometry. Apart from the Franck−Condon progressions that, based on the pump−probe spectroscopic results, are expected to underlie the line shape, other mechanisms should be responsible for this broadening. The low-frequency hydrogen bond modes that couple strongly to the O−H/O−D stretching modes are found to be underdamped and thus cannot account for the strong broadening.[166] Infrared photon-echo spectroscopy provides, as in the case of $HOD:D_2O$, insight into this problem.[129] In contrast to the line shape of the weakly hydrogen-bonded HOD, the decay of the macroscopic O−H/O−D stretching polarization is dominated by multilevel quantum beats, originating from the anharmonic coupling of the O−H/O−D stretching mode to several underdamped low-frequency modes of the hydrogen bonds. This is the conclusion drawn from experiments on the cyclic acetic acid dimer (the symmetric dimer $(CH_3COOH)_2$ and the mixed dimer $CD_3COOH-CD_3COOD$)[112,129] (Figure 21) and should also hold in retrospect for the previously studied system PMME-H.[106] The O−H stretching line shape of the cyclic acetic acid dimer results from transitions in a multilevel vibrational system. It is determined by anharmonic coupling to at least two low-frequency modes, of which the hydrogen bond stretching mode has a frequency dependent on the quantum state of the O−H stretching vibration. In addition, Fermi resonances with overtones or combination levels of the C−O, C═O, and O−H bending vibrations may contribute to the line shape,[21] as well as Davydov coupling between the O−H stretching oscillators. The interference of different nonlinear interaction pathways involving the anharmonically coupled low-frequency modes leads to a multilevel quantum beat. Due to the ≃1 ps dephasing time of the low-frequency coherences, such quantum beats give rise to the complex nonexponential decay and recurrences of the photon-echo signals. Theoretical calculations of the photon-echo signals which are based on a density matrix approach and take into account the low-frequency hydrogen bond modes at 50 and 150 cm^{-1} account for the experimental result.[129] Additional oscillatory contributions to the signal could be caused by macroscopic polarization beats due to the Davydov coupling of the two O−H stretching oscillators. In such a case, the electric fields radiated by the excitonically split polarizations on different molecules interfere on the detector and give rise to an additional oscillation with a frequency $\nu_{PI} = 2V_0/h$ (h is Planck's constant) that should be on the order of 50 cm^{-1}. The similarity of the photon-echo data for the symmetric dimer $(CH_3COOH)_2$ and the mixed dimer $CD_3COOH-CD_3COOD$, where Davydov coupling is absent, suggests that multilevel quantum beats dominate the overall polarization decay.

Three-pulse echo peak shift measurements (3PEPS) on PMME-H[106] and $(CH_3COOH)_2$[129] show a rapid decay within the pulse duration, after which negligible 3PEPS signal remains (Figure 21b). This indicates that additional inhomogeneous broadening processes can be discarded, as may be expected for these hydrogen-bonded systems with well-defined geometry. In contrast to the 3PEPS signal from HOD:D_2O, no additional interference effects occur due to the five-level system nature of the O−H stretching oscillator, since all phase memory is rapidly lost; i.e., the frequency fluctuation correlation function $C(t)$ has fully decayed within the first 200 fs.

Another feature shown by the 3PEPS signals is an oscillatory modulation by the coherently excited low-frequency hydrogen bond modes that are also responsible for the oscillatory contributions in the pump−probe signals. Coherent modulations of 3PEPS signals have been observed previously for electronic transitions of dye molecules in solution.[167,168] The wave packet motions of the coherently excited low-frequency modes modulate the shape of the three-pulse echo signals due to the quantum beats.[169] In the case of the modulations of the infrared 3PEPS signals, the same mechanism applies. When taking into account the effects of quantum beats and the fact that no additional significant inhomogeneity exists for the cyclic acetic acid dimer, a homogeneous dephasing time of $T_2 = 200 \pm 30$ fs is derived. This is found to be consistent with transient hole-burning results that show a spectral hole width of ≃50 cm^{-1}. Assuming a single transition to contribute to the spectral hole, one estimates a transverse dephasing time $T_2 = 1/(\pi\Gamma) \geq 200$ fs (Γ is the full width of spectral hole). If more than one transition contribute, the individual T_2 would be longer; i.e., hole burning allows for the estimation of a lower limit of T_2 only. The rather fast homogeneous dephasing can be caused by the combined effect of strong anharmonicity of the O−H

stretching mode and solvent fluctuations, in a line of argument similar to that used for HOD:D_2O.[57,67] In contrast to a small system such as HOD, however, one also has to consider for the larger acetic acid dimer or PMME-H/PMME-D the dephasing induced by higher-order coupling with other intramolecular modes. For instance, for PMME-D it has been shown that a coupling that is quadratic in the O−D stretching coordinate and linear in intra- and intermolecular modes leads to an ultrarapid dephasing on the order of 100 fs.[163,164]

6. Vibrational Energy Redistribution and Relaxation of O–H/O–D Stretching Vibrations

When a molecular vibration is excited, the molecular system responds to this nonequilibrium situation by redistributing the excess vibrational energy initially present in this vibration toward other modes (intramolecular vibrational energy redistribution, IVR) and by dissipation to the surrounding solvent modes (vibrational energy relaxation, VER). IVR and VER have been the subject of many studies for several decades, especially in the context of radiationless transitions of electronically excited states.[170,171] Here, after internal conversion to the electronic ground state, the interest lies in the VER process of excess energy to the solvent.[98,172,173] For isolated molecules in the gas phase, IVR can occur in the coherent limit if the initially excited vibronic state is coupled to a limited number of dark states. This results in intrinsic recurrences in populations of the excited states.[174,175]

Numerous studies on vibrational relaxation in the electronic ground state have been performed by use of time-resolved vibrational spectroscopic techniques, such as infrared-pump/infrared-probe, coherent anti-Stokes Raman scattering (CARS), and infrared-pump/anti-Stokes Raman-probe.[99,173,176−182] Much effort has been put into the investigation of VER of small (di- or triatomic) molecules in solution or in protein surroundings,[177,180] where a direct link with theoretical studies is the main target.[57,131,183,184] In hydrogen-bonded O−H/O−D stretching vibrations, IVR and VER have been studied extensively, and the typical time scales for such processes are much shorter than for other types of vibrations. A similar shortening of the relevant time scale was found for hydrogen-bonded pyrrole complexes.[185] IVR and VER in HOD:D_2O and H_2O will be discussed in section 6.1, where the main characteristics of population relaxation of hydrogen-bonded O−H/O−D stretching vibrations are presented. We then treat recent work on ions dissolved in water in section 6.2, and population relaxation in medium-strong hydrogen bonds in section 6.3. Work on alcohols is summarized in section 6.4.

6.1. Population Relaxation Dynamics in HOD:D_2O and H_2O

A large amount of work has been devoted to vibrational relaxation of O−H/O−D stretching modes in water. The first results on time-resolved infrared spectroscopy on the O−H stretching mode of HOD:D_2O were reported 12 years ago by Graener et al.[133] A lifetime of the O−H stretching mode of $T_1(\nu_{OH}) = 8 \pm 2$ ps was deduced from transient absorbance changes induced with 11 ps infrared pulses, conflicting with a saturation study with picosecond laser pulses by Vodopyanov,[186] where a value of $T_1(\nu_{OH}) = 0.5$ ps was derived. Today, the accepted value for HOD:D_2O is between 0.5 and 1 ps.[113−117,187−189] The O−H/O−D stretching mode lifetime depends on temperature. The T_1 value increases with temperature, being about twice as large in liquid D_2O as in solid D_2O ice.[187] The lifetime of the O−D stretching mode of HOD in H_2O is twice as long: $T_1(\nu_{OD}) = 1.8$ ps,[115,121,136] whereas the bending mode was estimated to have a lifetime of 0.6 ps $\leq T_1(\delta_{HOD}) \leq$ 1.2 ps.[136] The question now to be answered is how the vibrational energy of about 3400 cm^{-1} in the form of one O−H stretching quantum in HOD is redistributed/dissipated toward the other vibrational modes of HOD, to those of the solvent D_2O, and to the hydrogen bond modes (175 cm^{-1} stretching and 60 cm^{-1} bending).[30] In addition to the fundamental levels of these vibrations, also the $\delta_{OH} = 2$ overtone state has to be considered a relaxation pathway since it is often isoenergetic with the $\nu_{OH} = 1$ stretching state.

In the lifetime study by Nienhuys et al. on HOD:D_2O,[188] a transient blue-shifted absorption of the O−H stretching mode was found that appears with a time constant identical to the population relaxation time $T_1(\nu_{OH})$ of the initially excited O−H stretching $\nu_{OH} = 1$ state. Since this study, the five-level scheme of Figure 8 has often been used to describe the population relaxation dynamics of the O−H stretching vibration in hydrogen-bonded systems.[112,126,127,137,190−192] Nienhuys et al. argue that the hydrogen bond low-frequency modes are the main acceptors of the O−H stretching vibrational excitation energy. Due to the ultrafast relaxation, this excess energy is redistributed efficiently into these low-frequency modes, making them highly populated, with a weakening of the hydrogen bond as a consequence. The weakened hydrogen bond manifests itself through a transient O−H/O−D absorption that shows up blue-shifted compared to the original spectral position of the $\nu_{OH} = 0 \rightarrow 1$ transition. This blue-shifted band thus appears with a time constant identical to the $T_1(\nu_{OH})$ lifetime. Upon vibrational cooling due to energy dissipation to the solvent on a much longer time scale, the transient blue-shifted O−H/O−D stretching band decays on the order of several tens of picoseconds. The observed increase of $T_1(\nu_{OH})$ with temperature is ascribed to a decrease of hydrogen bond strength with temperature, making the anharmonic couplings between the O−H stretching mode and the hydrogen bond low-frequency modes weaker, where the latter function less efficiently as accepting modes.[187,188]

Although now the transient blue-shifted absorption has been observed in a large collection of molecular systems, the reason for the rapid O−H stretching population relaxation as given by Nienhuys et al. differs from conclusions of other groups, where the $\delta_{OH} = 2$ overtone state of the HOD bending mode is

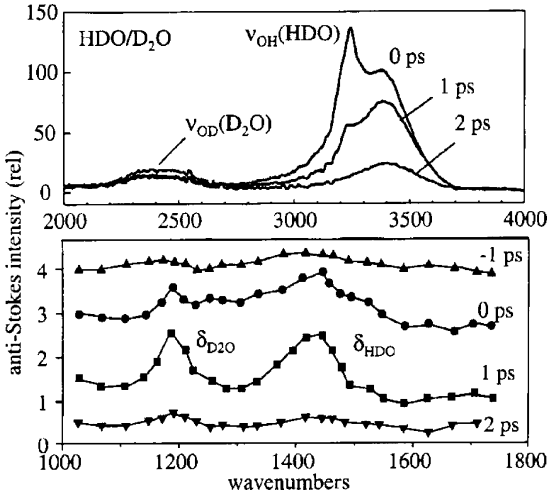

Figure 22. Anti-Stokes Raman transients for HOD in D_2O obtained after pumping the O−H stretching vibration. About 10% of the O−H excitation generates O−D stretching excitations after its decay. The spectra in the bending region show that equal amounts of bending excitations in HOD and D_2O are observed, with a quantum yield of the bending excitations via the stretching decay of $1.2 \leq \phi \leq 2.0$ (taken from ref 136).

assumed to couple the most efficiently with the O−H stretching vibration (Figure 6a). Gale et al. found a decrease of the O−H stretching excitation lifetime the closer the excitation occurred to the frequency position of this $\delta_{OH} = 2$ overtone state.[189] In addition, theoretical studies by Rey and Hynes[193] and by Lawrence and Skinner[45,194,195] have found that the $\nu_{OH} = 1 \rightarrow \delta_{OH} = 2$ pathway is actually an important one. We refer to the review paper by Rey, Møller, and Hynes for more details on the calculations of vibrational relaxation of HOD:D_2O.[196] The most direct experimental evidence that energy relaxation (at least partially) occurs through the bending vibrations is due to Deàk et al.,[136] who have studied the IVR and VER processes using infrared-pump/anti-Stokes Raman-probe spectroscopy (Figure 22). Here it was found that the bending vibration was excited with a quantum yield between $1.2 \leq \phi \leq 2.0$, meaning that relaxation through the bending vibration is the most important channel. Interestingly, excitation of the bending and stretching vibrations of the solvent D_2O was also detected, hinting at a rapid energy transfer to the solvent. Further studies have to be pursued to investigate whether the energy redistribution might occur to both bending overtone and low-frequency hydrogen bond modes, and what relative efficiencies and time scales are associated with these pathways. We note that the five-level scheme can be used as a general description of the population relaxation dynamics of O−H/O−D stretching vibrations, where the intermediate state is to be understood as being due to nonequilibrium excitations of any or a collection of the other vibrational modes in the molecular system. For HOD:D_2O these are the HOD bend, torsion, or hydrogen bond low-frequency modes or the low-frequency solvent continuum.

When the O−H concentration is increased to 1 M or more, a decrease of the rotational anisotropy decay has been ascribed to the effect of Förster resonant excitation energy transfer, through a dipole−dipole interaction mechanism, that is possible when H_2O molecules are nearest neighbors in the liquid. In the case of pure water, the anisotropy decay was found to be faster than 100 fs, from which Woutersen and Bakker conclude that interactions of higher order than dipole−dipole play a significant role.[197] Resonant intermolecular vibrational energy transfer between bilinearly coupled harmonic O−H stretching oscillators has been found, in a quantum mechanical wave packet study of clusters of water molecules in solid and liquid phases, to be responsible for such fast time scales.[198] In a more extended two-color pump−probe study,[137,190] Lock et al. revealed that the population relaxation in H_2O occurs with two characteristic time scales, 260 fs, which was attributed to T_1 population relaxation of the $\nu_{OH} = 1$ state at room temperature (increasing to 320 fs at 358 K), and 550 fs, attributed to thermalization where the $\nu_{OH} = 0'$ intermediate state relaxes back to the $\nu_{OH} = 0$ ground state. The faster T_1 relaxation time in H_2O compared to HOD:D_2O was ascribed to a better resonance condition for the $\delta_{OH} = 2$ overtone state in the case of H_2O. In contrast, Pakoulev et al. have deduced from an infrared-pump/anti-Stokes Raman-probe study that the process with the fast 0.26−0.32 ps time constant is due to a spectral diffusion process, and the population lifetime $T_1(\nu_{OH}) = 0.7$ ps.[199] In the latter study, several reasons have been given for the faster spectral diffusion process in H_2O (compare with the 0.5−1.0 ps time constant found for HOD:D_2O, see section 5.1). It can be due to faster breaking and formation times of hydrogen bonds since O−H···O bonds are weaker than O−D...O hydrogen bonds, the ν_{OH} frequency is affected by four hydrogen bonds rather than two in HOD:D_2O, and in experiments with H_2O the temperature jump due to the strong absorption of the infrared excitation pulse is much larger than that in HOD:D_2O.

A more detailed analysis of the O−H stretching and bending Raman bands of H_2O has led to the claim that the O−H stretch band can be decomposed into two sub-bands.[181,182] Vibrational relaxation in the larger red-shifted sub-band (with $T_1 = 0.55$ ps) occurs through the pathways $\nu_{OH} = 1 \rightarrow \delta_{OH} = 1$ (with a relative efficiency 1/3) and $\nu_{OH} = 1 \rightarrow \nu_{OH} = 0$ (with a relative efficiency 2/3). The blue-shifted sub-band ($T_1 = 0.75$ ps) decays predominantly via $\nu_{OH} = 1 \rightarrow \nu_{OH} = 0$. The bending $\delta_{OH} = 1$ state decays directly to the ground state with $T_1 = 1.4$ ps.

The influence of temperature, pressure, and the ice−water phase transition on the O−H stretching lifetime has been explored to some extent. Such phenomena are discussed in the review by Rey, Møller, and Hynes[196] and in ref 200.

6.2. Population Relaxation Dynamics of Water Molecules in Ion Solvation Shells

When ionic compounds are dissolved in water, a separation occurs between the ions due to solvation by water molecules. The interest here lies in the interaction mechanisms of solvation, where the possibility of hydrogen-bonding interactions in the solvation shells around the ions have to be characterized. Kropman and Bakker have measured the

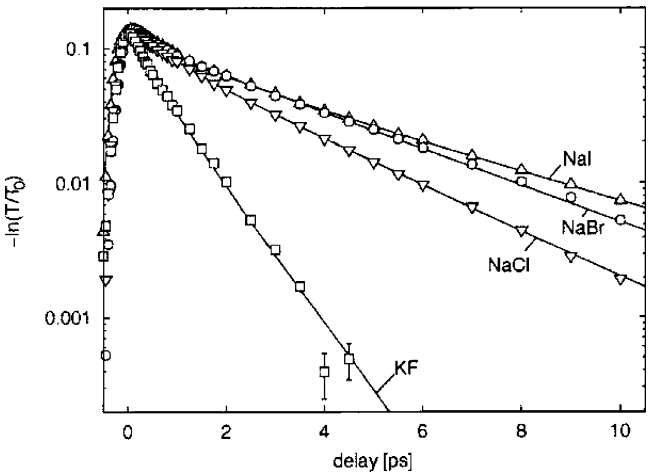

Figure 23. Room-temperature isotropic pump−probe scans of 6 M solutions of KF, NaCl, NaBr, and NaI, and biexponential fits describing the population relaxation. The pump frequency was 3450 cm^{-1}, and the probe frequency was 3200 cm^{-1}. For a solution of KF, the decay is almost identical to that of pure HOD:D_2O. Reproduced with permission from ref 203. Copyright 2003 Elsevier Science.

dynamics of O−H stretching bands of 0.1 M HOD:D_2O with added molar amounts of the salts KF, NaCl, NaBr, NaI, and $MgCl_2$.[201,202] They have found in infrared-pump/infrared-probe experiments that the addition of the salts leads to components in the response with long temporal characteristics, ascribed to the dynamics of HOD molecules in the first solvation shell around the ions. The vibrational lifetime of the O−H stretching mode of HOD in the proximity of an ion depends on the nature of the anion, with the largest value for I^-, whereas for F^- the lifetime is almost identical to that of bulk HOD: $T_1(\nu_{OH}) = 3.1$ (I^-), 2.9 (Br^-), 2.6 (Cl^-), and 0.8 ps (F^-) at 300 K[202,203] (Figure 23). In contrast, Laenen and Thaller have reported an extended lifetime of the O−H stretching mode with a value depending on the nature of the cation.[204−206] Kropman and Bakker have shown that the conclusions of Laenen and Thaller are erroneous due to insufficient detection sensitivity and that only the anion has a strong influence on the vibrational lifetime.[207] The temperature dependence of $T_1(\nu_{OH})$ of HOD bound in the solvation shell around an anion shows a decrease with temperature, in contrast to bulk HOD (see section 6.1). The facts that in transient hole-burning experiments spectral shifts have been detected with characteristic correlation times of 15−25 ps,[201,202] and that the anisotropy decay also has an extended temporal component of 12 ps,[208] indicate that the hydrogen-bonded network around the ion has less structural flexibility than in bulk water. From a determination of the orientational correlation time of water molecules in $Mg(ClO_4)_2$, $NaClO_4$, and Na_2SO_4 solutions, the conclusion has been drawn that these changes in the hydrogen-bonding network extend only to the nearest solvation shell, and that bulk water is not affected.[209] In the case of HOD molecules dissolved in a 10 M solution of NaOD:D_2O, the observed dynamics of the O−H stretching mode in an alkaline environment shows two components for the vibrational lifetime decay,[210] ascribed to HOD bound to D_2O ($T_1(\nu_{OH}) \simeq 600$ fs) and HOD bound to D_2O molecules or OD^- ions participating in proton transfers between HOD and OD^- or deuterium transfers between OD^- and D_2O ($T_1(\nu_{OH}) \simeq 160$ fs). The large difference in decay times indicates a slow exchange between the two components and is ascribed to a rigid hydrogen-bonded network.

6.3. Population Relaxation in Medium-Strong Hydrogen Bonds

The population relaxation dynamics of O−H/O−D stretching vibrations in medium-strong hydrogen bonds show a behavior similar to that of HOD:D_2O (see section 6.1). The observed features have been explained with the five-level scheme of Figure 8. A red-shifted excited-state absorption $\nu_{OH/OD} = 1 \rightarrow 2$ has been reported for PMME-D[125] and acetic acid dimer.[112,128,129,165] Blue-shifted transient absorption of the hot ground-state $\nu_{OH} = 0' \rightarrow 1'$ has been observed in the cases of PMME-H,[127] PMME-D,[125] HBT-D,[126] $(CD_3COOH)_2$,[165] $(CD_3COOH)_2$, $(CH_3COOD)_2$,[128] and $CD_3COOH-CD_3COOD$[129] (Figure 21). In all these studies, the population relaxation time of the O−H/O−D stretching mode is typically a fraction of the value for HOD:D_2O. The population relaxation appears for PMME-H and HBT-D to be ≤200 fs,[126,127] very close to the time resolution in these studies. For PMME-D, a value of $T_1(\nu_{OD}) \simeq 0.4$ ps has been given.[125] A very recent two-color pump−probe study of acetic acid dimers has given a lifetime of 200 fs for the $\nu = 1$ state of the O−H stretching oscillator.[211] We note that these values for acetic acid dimer are different from those found in an earlier study with a time resolution of 2.5, ps where a value $T_1(\nu_{OH}) \simeq 4$ ps was claimed.[165] For the O−H bending vibration, a lifetime of 250 fs was measured.[211] Clearly, more work has to be pursued to elucidate the population dynamics in the acetic acid dimer. After the population relaxation, the investigated molecular systems typically show a simultaneous decay of the $\nu_{OH/OD} = 0 \rightarrow 1$ ground-state bleach and hot ground-state absorption $\nu_{OH/OD} = 0' \rightarrow 1'$ on a time scale of 10−20 ps, indicating vibrational cooling by energy dissipation to the solvent.

A difference between weak and medium-strong hydrogen bonds is the stronger Fermi resonance interaction between the O−H/O−D stretching vibration and combination or overtone levels (in particular due to the O−H/O−D bending mode). The resulting infrared absorption line shapes for medium-strong hydrogen bonds show multipeak structures that may—at least partially—be due to level splittings by the Fermi resonances (Figure 6b).[21] In contrast to the population dynamics of O−H/O−D stretching modes in weak hydrogen bonds, where incoherent population decay to dark overtone levels is assumed, here it is more appropriate to consider the coherent picture, where the $\nu_{OH/OD} = 1$ stretching and the $\delta_{OH/OD} = 2$ bending levels mix strongly to form two optically allowed states.[175] Recurrences in population are not expected for condensed-phase systems due to the perturbing influence of the fluctuating solvent. Recent studies on the O−H/O−D stretching band of carboxylic acid dimers in the gas phase show the importance of Fermi resonances for the vibrational

line shape.[22,25,212−214] Revealing IVR dynamics of isolated carboxylic acid dimers will be important for comparison with the IVR dynamics in solution where the fluctuating solvent disturbs the phase of the O−H/O−D oscillator on a fast time scale. It should be noted that the room-temperature O−H band of acetic acid dimers in solution is broadened (cf. Figure 2), whereas gas-phase spectra of cold isolated dimers display narrow transition lines.[22] Moreover, the solvent can act as an additional acceptor of vibrational energy when the O−H/O−D stretching oscillator relaxes and the vibrational excesss energy is redistributed (see also ref 196).

Although experimental studies still have to be pursued to elucidate the vibrational couplings underlying IVR in medium-strong hydrogen bonds, theoretical work on medium-sized organic molecules such as PMME has indicated that one can treat the hydrogen bond vibrational system as consisting of the OH/OD stretching, bending, and hydrogen bond low-frequency modes that are strongly coupled to each other,[160−162] with the rest of the vibrational manifold as an intramolecular bath. These additional intramolecular modes, together with solvent modes, induce dephasing and vibrational relaxation on time scales <1 ps through higher-order coupling with the hydrogen bond vibrational system.[163,164,215]

6.4. Hydrogen Bond Cleavage in Alcohols

Alcohols form oligomers in nonpolar solvents, where the size of the complexes depends on the concentrations. The O−H/O−D stretching band shows several sub-bands due to internal hydrogen-bonded OH/OD groups, overlapping because of their bandwidth, as well as an isolated band due to terminal non-hydrogen-bonded O−H/O−D groups. We note here that the same transient spectral features are to be expected for hydrogen-bonded O−H/O−D vibrations, e.g., in HOD:D_2O (section 6.1) or in medium-strong hydrogen bonds (section 6.3). In other words, the red-shifted excited-state absorption and the blue-shifted transient absorption of the hot ground-state contribute to the pump−probe signals as defined for the five-level system in Figure 8. In alcohols, however, it has been argued that an additional relaxation path should occur: a channeling of the vibrational excitation energy into the hydrogen bond with a bond fission as a consequence.[216] This argument has been put forward on the basis of a comparison of the energy of one O−H stretching quantum with the hydrogen bond binding energy. Infrared-pump/infrared-probe spectroscopy of the O−H stretching band of hydrogen-bonded O−H groups has been performed on a variety of alcohols, ranging from silanols[217−219] and oligomers of methanol,[220] ethanol,[216,221−223] and sterically hindered 2,2-dimethyl-3-ethyl-3-pentanol[224−226] in nonpolar solvents to ethanol in deuterated ethanol.[227] From these studies, a fast relaxation time for hydrogen-bonded O−H stretching vibrations has been found ($T_1(\nu_{OH}) \simeq 0.45-0.6$ ps for methanol;[220] note that longer lifetimes have been derived for ethanol in studies with longer pulse durations[222]), much shorter than that of a non-hydrogen-bonded O−H groups, where the lifetime $T_1(\nu_{OH}) \simeq 8$ ps.[228] Recombination time scales after hydrogen bond cleavage are reported to be on the order of 9 ps for methanol.[220] The excitation dynamics of the C−O stretching vibration of methanol and ethanol monomers has also been studied, where a lifetime of 3.2 ps has been derived from the data.[191] Recent studies of the OD stretching band of oligomers of methanol-*d*, ethanol-*d*, and 1-propanol-*d* in nonpolar solution have concentrated on the energy transfer after excitation of the terminal non-hydrogen-bonded O−D group[229,230] and of the hydrogen-accepting and -donating O−D groups.[231,232] A kinetic model has been used to fit spectrally integrated signals, from which hydrogen bond breaking and recombination times have been derived. An infrared photon-echo study has shown that frequency correlation exists between the initially excited O−D stretching vibration and the frequency-shifted O−D stretching band formed by hydrogen bond breaking.[233] Polarization-dependent studies have shown an orientational relaxation faster than 200 fs in the case of ethanol, ascribed to a fast O−H excitation transfer over the oligomer.[223] Orientational relaxation of isolated O−D stretching vibrations of deuterated methanol within oligomers has shown rotational diffusion contributions with 1.7 and 17 ps time constants, whereas the fast decay on subpicosecond time scales in isotopically pure methanol-*d* oligomers indicates the vibrational excitation transfer.[234]

Vibrational energy transfer of alcohols after excitation of the C−H stretching[235,236] and the O−H stretching modes has also been investigated.[237] In particular, the infrared-pump/anti-Stokes Raman-probe technique clearly shows how energy is redistributed among the different vibrational modes.[238] In particular, the OH stretching excitation appears to be redistributed among all other modes, whereas redistribution after CH stretching excitation follows a more direct pathway.[236,237]

7. Conclusions and Prospects

The extensive experimental and theoretical work reviewed here demonstrates the potential of nonlinear vibrational spectroscopy for reaching a microscopic understanding of hydrogen bonds in liquids. This field is of substantial current interest, with new developments in ultrafast technology and spectroscopy, e.g., toward multidimensional methods, and an extension of research to complex hydrogen-bonded systems going on. A number of important generalized conclusions result from the work performed so far:

(i) O−H and O−D stretching excitations in weak hydrogen bonds display vibrational dephasing and spectral diffusion in the subpicosecond time domain, with the fastest decay components in the sub-100 fs regime. The fast dephasing is markedly different from that of free O−H/O−D stretching vibrators and is linked to the enhanced anharmonicity of the hydrogen-bonded oscillators, which makes them more sensitive to the fluctuating forces exerted by the liquid environment. Theoretical molecular dynamics simulations of HOD in D_2O, considering vibrational three-level systems in a fluctuating environment, account for this fast dephasing. Two- and three-pulse

photon-echo studies and molecular dynamics simulations have provided insight into the frequency fluctuation correlation function of this system, and a number of fast femtosecond and slower picosecond components have been derived. The interpretation of such results is still somewhat conflicting.

(ii) The dynamics of coherent O−H stretching excitations in medium-strong hydrogen bonds is strongly influenced by the multilevel character of the vibrational system resulting from anharmonic coupling to low-frequency modes. This coupling leads to multilevel coherences strongly affecting the decay of the macrosopic coherent polarization. For cyclic dimers of acetic acid, the O−H/O−D stretching bands consist of progressions of homogeneously broadened lines with a 200 fs dephasing time and negligible inhomogeneous broadening. As a result, spectral diffusion is practically absent.

(iii) Low-frequency wave packet motions along underdamped hydrogen bond modes have been induced via ultrafast broadband excitation of the O−H/O−D stretching oscillators in medium-strong intra- and intermolecular hydrogen bonds. Such motions, which modulate the length and the strength of the hydrogen bonds, are damped with picosecond dephasing times, i.e., much slower than the coherence decay on the O−H/O−D stretching oscillators.

(iv) The population lifetimes of hydrogen-bonded O−H/O−D stretching oscillators are subpicosecond, in a range from about 200 fs for medium-strong to nearly 1 ps for weak hydrogen bonds. The pathways of population relaxation are understood only in part; both Fermi resonances with overtones and combination tones, including in particular the O−H/O−D bending modes, and the coupling to low-frequency hydrogen bond modes seem to be relevant. The dissipation of vibrational excess energy results in the formation of a hot ground state characterized by a blue-shifted O−H/O−D stretching absorption. Eventually, the hot ground state cools by energy transfer to the surrounding liquid within tens of picoseconds.

(v) Cleavage and re-formation of weak hydrogen bonds occur in the subpico- to picosecond time domain and are thus relevant for the relaxation of vibrational excitations.

The extension of such studies from liquids to biologically relevant systems such as hydrogen bonds in proteins represents an important direction of research which will help to unravel the structure−function relationships of biomolecules. In addition, ultrafast hydrogen bond dynamics is highly relevant for hydrogen- and proton-transfer processes both in the electronic ground state and in vibronically excited molecules. The observation of comparably long-lived coherences in low-frequency hydrogen bond modes may help to implement optical control of such reactions by interaction with coherent infrared pulses and/or pulse sequences.

8. Acknowledgment

We would like to thank Jens Stenger, Dorte Madsen, Nils Huse, Karsten Heyne, Jens Dreyer, and Peter Hamm for their important contributions to part of the work reviewed here. Financial support by the Deutsche Forschungsgemeinschaft and the Fonds der Chemischen Industrie is gratefully acknowledged. We thank H. J. Bakker, D. D. Dlott, J. T. Hynes, and J. L. Skinner for making possible the reproduction of Figures 3, 14, 16, 22, and 23, and in addition J. T. Hynes and K. B. Møller for sending us a preprint of ref 196.

9. References

(1) Schuster, P., Zundel, G., Sandorfy, C., Eds. *The hydrogen bond: Recent developments in theory and experiments*; North-Holland: Amsterdam, 1976; Vols. I−III.
(2) Elsaesser, T., Bakker, H. J., Eds. *Ultrafast hydrogen bonding dynamics and proton transfer processes in the condensed phase*; Kluwer: Dordrecht, 2002.
(3) Fayer, M. D., Ed. *Ultrafast infrared and Raman spectroscopy*; Marcel Dekker: New York, 2001.
(4) Zwier, T. S. *Annu. Rev. Phys. Chem.* **1996**, *47*, 205.
(5) Robertson, W. H.; Johnson, M. A. *Annu. Rev. Phys. Chem.* **2003**, *54*, 173.
(6) Buck, U.; Huisken, F. *Chem. Rev* **2000**, *100*, 3863.
(7) Buck, U.; Huisken, F. *Chem. Rev.* **2001**, *101*, 205.
(8) Elsaesser, T. In ref 2, p 119.
(9) Douhal, A.; Lahmani, F.; Zewail, A. *Chem. Phys.* **1996**, *207*, 477.
(10) Sandorfy, C. In ref 1, Vol. II, Chapter 13, p 613.
(11) Buckingham, A. D. In *Theoretical treatments of hydrogen bonding*; Hadži, D., Ed.; Wiley: New York 1997; p 1.
(12) Hadži, D.; Bratos, S. In ref 1, Vol. II, Chapter 12, p 565.
(13) Novak, A. *Struct. Bonding (Berlin)* **1974**, *18*, 177.
(14) Mikenda, W. *J. Mol. Struct.* **1986**, *147*, 1.
(15) Bratos, S. *J. Chem. Phys.* **1975**, *63*, 3499.
(16) Bratos, S.; Leicknam J. C.; Gallot, G.; Ratajczak, H. In ref 2, p 5.
(17) Marechal, Y.; Witkowski, A. *J. Chem. Phys.* **1968**, *48*, 3697.
(18) Redington, R. L.; Lin, K. C. *J. Chem. Phys.* **1971**, *54*, 4111.
(19) Bertie, J. E.; Michaelian, K. H. *J. Chem. Phys.* **1982**, *76*, 886.
(20) Bertie, J. E.; Michaelian, K. H. *J. Chem. Phys.* **1982**, *77*, 5267.
(21) Maréchal, Y. *J. Chem. Phys.* **1987**, *87*, 6344.
(22) Häber, T.; Schmitt, U.; Emmeluth, C.; Suhm, M. A. *Faraday Discuss.* **2001**, *118*, 331.
(23) Chamma, D.; Henri-Rousseau, O. *Chem. Phys.* **1999**, *248*, 53.
(24) Chamma, D.; Henri-Rousseau, O. *Chem. Phys.* **1999**, *248*, 71.
(25) Florio, G. M.; Zwier, T. S.; Myshakin, E. M.; Jordan, K. D.; Sibert, E. L., III. *J. Chem. Phys.* **2003**, *118*, 1735.
(26) Mikenda, W.; Steinböck, S. *J. Mol. Struct.* **1996**, *384*, 159.
(27) Rey, R.; Møller, K. B.; Hynes, J. T. *J. Phys. Chem. A* **2002**, *106*, 11993.
(28) Lawrence, C. P.; Skinner, J. L. *J. Chem. Phys.* **2003**, *118*, 264.
(29) Montrose, C. J.; Bucaro, J. A.; Litovitz, T. A.; Marshall-Coakley, J. *J. Chem. Phys.* **1974**, *60*, 5025.
(30) Castner, E. W., Jr.; Chang, Y. J.; Chu, Y. C.; Walrafen, G. E. *J. Chem. Phys.* **1995**, *102*, 653.
(31) Kearley, G. J.; Fillaux, F.; Baron, M. H.; Bennington, S.; Tomkinson, J. *Science* **1994**, *264*, 1285.
(32) Rønne, C.; Astrand, P. O.; Keiding, S. R. *Phys. Rev. Lett.* **1999**, *82*, 2888.
(33) Rønne, C.; Keiding, S. R. *J. Mol. Liq.* **2002**, *101*, 199.
(34) Mizoguchi, K.; Hori, A.; Tominaga, Y. *J. Chem. Phys.* **1992**, *97*, 1961.
(35) Fujii, Y.; Yamada, H.; Mizuta, M. *J. Phys. Chem.* **1988**, *92*, 6768.
(36) Faurskov-Nielsen, O.; Lund, P. A. *J. Chem. Phys.* **1983**, *78*, 652.
(37) Nakabayashi, T.; Kosugi, K.; Nishi, N. *J. Phys. Chem. A* **1999**, *103*, 8595.
(38) Zelsmann, H. R.; Mielke, Z.; Marechal, Y. *J. Mol. Struct.* **1990**, *237*, 273.
(39) Gordon, R. G. *Adv. Magn. Reson.* **1968**, *3*, 1.
(40) Henri-Rousseau, O.; Blaise, P. *Adv. Chem. Phys.* **1998**, *103*, 1.
(41) Lippincott, E. R.; Schroeder, R. *J. Chem. Phys.* **1955**, *23*, 1099.
(42) Reid, C. *J. Chem. Phys.* **1959**, *30*, 182.
(43) Ibers, J. A. *J. Chem. Phys.* **1964**, *41*, 25.
(44) Polyansky, O. L.; Jensen, P.; Tennyson, J. *J. Chem. Phys.* **1996**, *105*, 6490.
(45) Lawrence, C. P.; Skinner, J. L. *J. Chem. Phys.* **2002**, *117*, 5827.
(46) Lawrence, C. P.; Skinner, J. L. *J. Chem. Phys.* **2002**, *117*, 8847.
(47) Stepanov, B. I. *Nature* **1946**, *157*, 808.
(48) Henri-Rousseau, O.; Blaise, P.; Chamma, D. *Adv. Chem. Phys.* **2002**, *121*, 241.
(49) Lim, M.; Hochstrasser, R. M. *J. Chem. Phys.* **2001**, *115*, 7629.
(50) Janoschek, R.; Weidemann, G.; Zundel, G. *J. Chem. Soc., Faraday Trans. 2* **1973**, *69*, 505.
(51) Rösch, N.; Ratner, M. *J. Chem. Phys.* **1974**, *61*, 3344.
(52) Robertson, G. N.; Yarwood, J. *Chem. Phys.* **1978**, *32*, 267.
(53) Boulil, B.; Henri-Rousseau, O.; Blaise, P. *Chem. Phys.* **1988**, *126*, 263.

(54) Diraison, M.; Guissani, Y.; Leicknam, J.-C.; Bratos, S. *Chem. Phys. Lett.* **1996**, *258*, 348.
(55) Mukamel, S. *Principles of nonlinear optical spectroscopy*; Oxford University Press: Oxford, 1995
(56) Hamm, P.; Hochstrasser, R. M. In ref 3, p 273.
(57) Oxtoby, D. W.; Levesque, D.; Weis, J. J. *J. Chem. Phys.* **1978**, *68*, 5528.
(58) Oxtoby, D. W. *Adv. Chem. Phys.* **1979** *40*, 1,
(59) Levesque, D.; Weis, J. J.; Oxtoby, D. W. J. *Chem. Phys.* **1980**, *72*, 2744.
(60) Bratos, S.; Leicknam, J.-Cl. *J. Chem. Phys.* **1994** *101*, 4536.
(61) Bratos, S.; Leicknam, J.-Cl. *J. Mol. Liq.* **1995**, *64*, 151.
(62) Bratos, S.; Leicknam, J.-Cl. *J. Chem. Phys.* **1995**, *103*, 4887.
(63) Williams, R. B.; Loring, R. F. *J. Chem. Phys.* **2000**, *113*, 1932.
(64) Williams, R. B.; Loring, R. F. *J. Chem. Phys.* **2000**, *113*, 10651.
(65) Williams, R. B.; Loring, R. F. *Chem. Phys.* **2001**, *266*, 167.
(66) Akiyama, R.; Loring, R. F. *J. Chem. Phys.* **2002**, *116*, 4655.
(67) Stenger, J.; Madsen, D.; Hamm, P.; Nibbering, E. T. J.; Elsaesser, T. *J. Phys. Chem. A* **2002**, *106*, 2341.
(68) Kubo, R. *Adv. Chem. Phys.* **1969** *15*, 101.
(69) Wynne, K.; Hochstrasser, R. M. *Chem. Phys.* **1995**, *193*, 211.
(70) Hamm, P. *Chem. Phys.* **1995**, *200*, 415.
(71) Shen, Y. R. *The principles of nonlinear optics*; Wiley: New York, 1984, Chapter 5.
(72) Dmitriev, V. G.; Gurzadyan, G. G.; Nikogosyan, D. N. *Handbook of nonlinear optical crystals*; Springer-Verlag: Berlin, 1991.
(73) Weiner, A. M. *IEEE J. Quantum Electron.* **1983**, *19*, 1276.
(74) Joffre, M.; Bonvalet, A.; Migus, A.; Martin, J. L. *Opt. Lett.* **1996**, *21*, 964.
(75) Bonvalet, A.; Joffre, M.; Martin, J. L.; Migus, A. *Appl. Phys. Lett.* **1995**, *67*, 2907.
(76) Kaindl, R. A.; Smith, D. C.; Joschko, M.; Hasselbeck, M. P.; Woerner, M.; Elsaesser, T. *Opt. Lett.* **1998**, *23*, 861.
(77) Kaindl, R. A.; Eickemeyer, F.; Woerner, M.; Elsaesser, T. *Appl. Phys. Lett.* **1999**, *75*, 1060.
(78) Huber, R.; Brodschelm, A.; Tauser, F.; Leitenstorfer, A. *Appl. Phys. Lett.* **2000**, *76*, 3191.
(79) Wachman, E. S.; Edelstein, D. C.; Tang, C. L. *Opt. Lett.* **1990**, *15*, 136.
(80) Fu, Q.; Mak, G.; van Driel, H. M. *Opt. Lett.* **1992**, *17*, 1006.
(81) Burr, K. C.; Tang, C. L.; Arbore, M. A.; Fejer, M. M. *Opt. Lett.* **1997**, *22*, 1458.
(82) Lohner, A.; Kruck, P.; Rühle, W. W. *Appl. Phys. B* **1994**, *59*, 211.
(83) Fraser, J. M.; Wang, D.; Hache, A.; Allan, G. R.; van Driel, H. M. *Appl. Opt.* **1997**, *36*, 5044.
(84) Ehret, S.; Schneider, H. *Appl. Phys. B* **1998**, *66*, 27.
(85) Wu, Q.; Zhang, X. C. *Appl. Phys. Lett.* **1997**, *71*, 1285.
(86) Gruetzmacher, J. A.; Scherer, N. P. *Rev. Sci. Instrum.* **2002**, *73*, 2227.
(87) For a recent overview, see: Bosenberg, W. R., Eckardt, R. C., Eds. *J. Opt. Soc. Am. B* **1995**, *12*, special issue on parametric devices, p 2084.
(88) Seifert, F.; Petrov, V.; Woerner, M. *Opt. Lett.* **1994**, *19*, 2009.
(89) Kaindl, R. A.; Wurm, M.; Reimann, K.; Hamm, P.; Weiner, A. M.; Woerner, M. *J. Opt. Soc. Am. B* **2000**, *17*, 2086.
(90) Hamm, P.; Kaindl, R. A.; Stenger, J. *Opt. Lett.* **2000**, *25*, 1798.
(91) Eickemeyer, F.; Kaindl, R. A.; Woerner, M.; Elsaesser, T.; Weiner, A. M. *Opt. Lett.* **2000**, *25*, 1472.
(92) Witte, T.; Zeidler, D.; Proch, D.; Kompa, K. L.; Motzkus, M. *Opt. Lett.* **2002**, *27*, 131.
(93) Belabas, N.; Likforman, J. P.; Canioni, L.; Bousquet, B.; Joffre, M. *Opt. Lett.* **2001**, *26*, 743.
(94) Tan, H. S.; Schreiber, E.; Warren, W. S. *Opt. Lett.* **2002**, *27*, 439.
(95) Reimann, K.; Smith, R. P.; Weiner, A. M.; Elsaesser, T.; Woerner, M. *Opt. Lett.* **2003**, *28*, 471.
(96) Knippels, G. M. H.; Mols, R. F. X. A. M.; van der Meer, A. F. G.; Oepts, D.; van Amersfoort, P. W. *Phys. Rev. Lett.* **1995**, *75*, 1755.
(97) Knippels, G. M. H.; van de Pol, M. J.; Pellemans, H. P. M.; Planken, P. C. M.; van der Meer, A. F. G. *Opt. Lett.* **1998**, *23*, 1754.
(98) Seilmeier, A.; Kaiser, W. In *Ultrashort laser pulses. Generation and applications*, 2nd ed.; Kaiser, W., Ed.; Topics in Applied Physics 60; Springer: Berlin, 1993; p 279.
(99) Dlott, D. D. *Chem. Phys.* **2001**, *266*, 149.
(100) Pollard, W. T.; Mathies, R. A. *Annu. Rev. Phys. Chem.* **1992**, *43*, 497.
(101) Mukamel, S. *Annu. Rev. Phys. Chem.* **2000**, *51*, 691.
(102) Moran, A. M.; Park, S. M.; Dreyer, J.; Mukamel, S. *J. Chem. Phys.* **2003**, *118*, 3651.
(103) Fleming, G. R.; Cho, M. *Annu. Rev. Phys. Chem.* **1996** *47*, 109.
(104) de Boeij, W. P.; Pshenichnikov, M. S.; Wiersma, D. A. *Annu. Rev. Phys. Chem.* **1998**, *49*, 99.
(105) Stenger, J.; Madsen, D.; Hamm, P.; Nibbering, E. T. J.; Elsaesser, T. *Phys. Rev. Lett.* **2001**, *87*, 027401.
(106) Stenger, J.; Madsen, D.; Dreyer, J.; Hamm, P.; Nibbering, E. T. J.; Elsaesser, T. *Chem. Phys. Lett.* **2002**, *354*, 256.
(107) Yeremenko, S.; Pshenichnikov, M. S.; Wiersma, D. A. *Chem. Phys. Lett.* **2003**, *369*, 107.
(108) Scheurer, C.; Piryatinski, A.; Mukamel, S. *J. Am. Chem. Soc.* **2001**, *123*, 3114.
(109) Joo, T.; Jia, Y.; Yu, J.-Y.; Lang, M. J.; Fleming, G. R. *J. Chem. Phys.* **1996**, *104*, 6089.
(110) de Boeij, W. P.; Pshenichnikov, M. S.; Wiersma, D. A. *Chem. Phys. Lett.* **1996**, *253*, 53.
(111) Fecko, C. J.; Eaves, J. D.; Loparo, J. J.; Tokmakoff, A.; Geissler, P. L. *Science* **2003**, *301*, 1698.
(112) Heyne, K.; Huse, N.; Nibbering, E. T. J.; Elsaesser, T. *J. Phys.: Condens. Mater.* **2003**, *15*, S129.
(113) Laenen, R.; Rauscher, C.; Laubereau, A. *Phys. Rev. Lett.* **1998**, *80*, 2622.
(114) Laenen, R.; Rauscher, C.; Laubereau, A. *J. Phys. Chem. B* **1998**, *102*, 9304.
(115) Laenen, R.; Simeonidis, K.; Laubereau, A. *J. Phys. Chem. B* **2002**, *106*, 408.
(116) Laenen, R.; Simeonidis, K.; Laubereau, A. *Bull. Chem. Soc. Jpn.* **2002**, *75*, 925.
(117) Gale, G. M.; Gallot, G.; Hache, F.; Lascoux, N.; Bratos, S.; Leicknam, J.-Cl. *Phys. Rev. Lett.* **1999**, *82*, 1068.
(118) Bratos, S.; Gale, G. M.; Gallot, G.; Hache, F.; Lascoux, N.; Leicknam, J.-Cl. *Phys. Rev. E* **2000**, *61*, 5211.
(119) Gallot, G.; Lascoux, N.; Gale, G. M.; Leicknam, J.-Cl.; Bratos, S.; Pommeret, S. *Chem. Phys. Lett.* **2001**, *341*, 535.
(120) Woutersen, S.; Bakker, H. J. *Phys. Rev. Lett.* **1999**, *83*, 2077.
(121) Kropman, M. F.; Nienhuys, H.-K.; Woutersen, S.; Bakker, H. J. *J. Phys. Chem. A* **2001**, *105*, 4622.
(122) Bakker, H. J.; Nienhuys, H.-K.; Gallot, G.; Lascoux, N.; Gale, G. M.; Leicknam, J.-Cl.; Bratos, S. *J. Chem. Phys.* **2002**, *116*, 2592.
(123) Piryatinski, A.; Lawrence, C. P.; Skinner, J. L. *J. Chem. Phys.* **2003**, *118*, 9664.
(124) Piryatinski, A.; Lawrence, C. P.; Skinner, J. L. *J. Chem. Phys.* **2003**, *118*, 9672.
(125) Stenger, J.; Madsen, D.; Dreyer, J.; Nibbering, E. T. J.; Hamm, P.; Elsaesser, T. *J. Phys. Chem. A* **2001**, *105*, 2929.
(126) Madsen, D.; Stenger, J.; Dreyer, J.; Nibbering, E. T. J.; Hamm, P.; Elsaesser, T. *Chem. Phys. Lett.* **2001**, *341*, 56.
(127) Madsen, D., Stenger, J., Dreyer, J., Hamm, P., Nibbering, E. T. J.; Elsaesser, T. *Bull. Chem. Soc. Jpn.* **2002**, *75*, 909.
(128) Heyne, K.; Huse, N.; Nibbering, E. T. J.; Elsaesser, T. *Chem. Phys. Lett.* **2003**, *369*, 591.
(129) Huse, N.; Heyne, K.; Dreyer, J.; Nibbering, E. T. J.; Elsaesser, T. *Phys. Rev. Lett.* **2003**, *91*, 197401.
(130) Zimdars, D.; Tokmakoff, A.; Chen, S.; Greenfield, S. R.; Fayer, M. D.; Smith, T. I.; Schwettman, H. A. *Phys. Rev. Lett.* **1993**, *70*, 2718.
(131) Rey, R.; Hynes, J. T. *J. Chem. Phys.* **1998**, *108*, 142.
(132) Graener, H.; Seifert, G. *J. Chem. Phys.* **1993**, *98*, 36.
(133) Graener, H.; Seifert, G.; Laubereau, A. *Phys. Rev. Lett.* **1991**, *66*, 2092.
(134) Woutersen, S.; Bakker, H. J. *J. Opt. Soc. Am. B* **2000**, *17*, 827.
(135) Hamm, P.; Lim, M.; Hochstrasser, R. M. *Phys. Rev. Lett.* **1998**, *81*, 5326.
(136) Deàk, J. C.; Rhea, S. T.; Iwaki, L. K.; Dlott, D. D. *J. Phys. Chem. A* **2000**, *104*, 4866.
(137) Lock, A. J.; Woutersen, S.; Bakker, H. J. *J. Phys. Chem. A* **2001**, *105*, 1238.
(138) Woutersen, S.; Emmerichs, U.; Bakker, H. J. *Science* **1997**, *278*, 658.
(139) Nienhuys, H.-K.; van Santen, R. A.; Bakker, H. J. *J. Chem. Phys.* **2000**, *112*, 8487.
(140) Bakker, H. J.; Woutersen, S.; Nienhuys, H. K. *Chem. Phys.* **2000**, *258*, 233.
(141) Gallot, G.; Bratos, S.; Pommeret, S.; Lascoux, N.; Leicknam, J.-Cl.; Kozinski, M.; Amir, W.; Gale, G. M. *J. Chem. Phys.* **2002**, *117*, 11301.
(142) Mountain, R. D. *J. Chem. Phys.* **1995**, *103*, 3084.
(143) Luzar, A.; Chandler, D. *Nature* **1996**, *379*, 55.
(144) Luzar, A.; Chandler, D. *Phys. Rev. Lett.* **1996**, *76*, 928.
(145) Martí, J.; Padró, J. A.; Guàrdia, E. *J. Chem. Phys.* **1996**, *105*, 639.
(146) Ohmine, I.; Saito, S. *Acc. Chem. Res.* **1999**, *32*, 741.
(147) Starr, F. W.; Nielsen, J. K.; Stanley, H. E. *Phys. Rev. Lett.* **1999**, *82*, 2294.
(148) Starr, F. W.; Sastry, S.; La Nave, E.; Scala, A.; Stanley, H. E.; Sciortino, F. *Phys. Rev. E* **2001**, *63*, 041201.
(149) Giovambattista, N.; Starr, F. W.; Sciortino, F.; Buldyrev, S. V.; Stanley, H. E. *Phys. Rev. E* **2002**, *65*, 041502.
(150) Lawrence, C. P.; Skinner, J. L. *Chem. Phys. Lett.* **2003**, *369*, 472.
(151) Dougherty, T. P.; Wiederrecht, G. P.; Nelson, K. A.; Garrett, M. H.; Jensen, H. P.; Warde, C. *Science* **1992**, *258*, 770.
(152) Rosker, M. J.; Wise, F. W.; Tang, C. L. *Phys. Rev. Lett.* **1986**, *57*, 321.
(153) Zewail, A. H. *Science* **1988**, *242*, 1645.
(154) Fragnito, H. L.; Bigot, J. Y.; Becker, P. C.; Shank, C. V. *Chem. Phys. Lett.* **1989**, *160*, 101.
(155) Dantus, M.; Bowman, R. M.; Gruebele, M.; Zewail, A. H. *J. Chem. Phys.* **1989**, *91*, 7437.

(156) Pugliano, N.; Palit, D. K.; Szarka, A. Z.; Hochstrasser, R. M. *J. Chem. Phys.* **1993**, *99*, 7273.
(157) Wang, Q.; Schoenlein, R. W.; Peteanu, L. A.; Mathies, R. A.; Shank, C. V. *Science* **1994**, *266*, 422.
(158) Zhu, L.; Sage, J. T.; Champion, P. M. *Science* **1994**, *266*, 629.
(159) Kumar, A. T. N.; Rosca, F.; Widom, A.; Champion, P. M. *J. Chem. Phys.* **2001**, *114*, 701.
(160) Paramonov, G. K.; Naundorf, H.; Kühn, O. *Eur. Phys. J. D* **2001**, *14*, 205.
(161) Naundorf, H.; Kühn, O. In *Femtochemistry and Femtobiology*; Douhal, A., Santamaria, J., Eds.; World Scientific: Singapore, 2002; p 438.
(162) Naundorf, H.; Worth, G. A.; Meyer, H.-D.; Kühn, O. *J. Phys. Chem. A* **2002**, *106*, 719.
(163) Kühn, O. *J. Phys. Chem. A* **2002**, *106*, 7671.
(164) Kühn, O.; Naundorf, H. *Phys. Chem. Chem. Phys.* **2003**, *5*, 79.
(165) Seifert, G.; Patzlaff, T.; Graener, H. *Chem. Phys. Lett.* **2001**, *333*, 248.
(166) Blaise, P.; Henri-Rousseau, O.; Grandjean, A. *Chem. Phys.* **1999**, *244*, 405.
(167) Passino, S. A.; Nagasawa, Y.; Joo, T.; Fleming, G. R. *J. Phys. Chem. A* **1997**, *101*, 725.
(168) Passino, S. A.; Nagasawa, Y.; Fleming, G. R. *J. Chem. Phys.* **1997**, *107*, 6094.
(169) de Boeij, W. P.; Pshenichnikov, M. S.; Wiersma, D. A. *J. Phys. Chem.* **1996**, *100*, 11806.
(170) Kommandeur, J.; Majewski, W. A.; Meerts, W. L.; Pratt, D. W. *Annu. Rev. Phys. Chem.* **1987**, *38*, 433.
(171) Kommandeur, J. *Adv. Chem. Phys.* **1987**, *70* (1), 133.
(172) Diestler, D. J. In *Radiationless processes in molecules and condensed phases*; Fong, F. K., Ed.; Topics in Applied Physics 15; Springer: Berlin, 1976; p 169.
(173) Elsaesser, T.; Kaiser, W. *Annu. Rev. Phys. Chem.* **1991**, *42*, 83.
(174) Felker, P. M.; Zewail, A. H. In *Jet spectroscopy and molecular dynamics*; Hollas, J. M., Phillips, D., Eds.; Chapman & Hall: Glasgow, 1995; p 222.
(175) Gruebele, M. Adv. *Chem. Phys.* **2000**, *114*, 193.
(176) Laubereau, A.; Kaiser, W. *Rev. Mod. Phys.* **1978**, *50*, 607.
(177) Owrutsky, J. C.; Raftery, D.; Hochstrasser, R. M. *Annu. Rev. Phys. Chem.* **1994**, *45*, 519.
(178) Deàk, J. C.; Iwaki, L. K.; Rhea, S. T.; Dlott, D. D. *J. Raman Spectrosc.* **2000**, *31*, 263.
(179) Iwaki, L. K.; Deàk, J. C.; Rhea, S. T.; Dlott, D. D. In ref 3, p 541.
(180) Myers, D. J.; Shigeiwa, M.; Fayer, M. D.; Cherayil, B. J. In ref 3, p 625.
(181) Wang, Z.; Pakoulev, A.; Pang, Y.; Dlott, D. D. *Chem. Phys. Lett.* **2003**, *378*, 281.
(182) Pakoulev, A.; Wang, Z.; Pang, Y.; Dlott, D. D. *Chem. Phys. Lett.* **2003**, *380*, 404.
(183) Hynes, J. T.; Rey, R. In ref 3, p 593.
(184) Skinner, J. L.; Egorov, S. A.; Everitt, K. F. In ref 3, p 675.
(185) Grubbs, W. T.; Dougherty, T. P.; Heilweil, E. J. *J. Phys. Chem.* **1995**, *99*, 10716.
(186) Vodopyanov, K. L. *J. Chem. Phys.* **1991**, *94*, 5389.
(187) Woutersen, S.; Emmerichs, U.; Nienhuys, H.-K.; Bakker, H. J. *Phys. Rev. Lett.* **1998**, *81*, 1106.
(188) Nienhuys, H.-K.; Woutersen, S.; van Santen, R. A.; Bakker, H. J. *J. Chem. Phys.* **1999**, *111*, 1494.
(189) Gale, G. M.; Gallot, G.; Lascoux, N. *Chem. Phys. Lett.* **1999**, *311*, 123.
(190) Lock, A. J.; Bakker, H. J. *J. Chem. Phys.* **2002**, *117*, 1708.
(191) van den Broek, M. A. F. H.; Nienhuys, H.-K.; Bakker, H. J. *J. Chem. Phys.* **2001**, *114*, 3182.
(192) van den Broek, M. A. F. H.; Kropman, M. F.; Bakker, H. J. *Chem. Phys. Lett.* **2002**, *357*, 8.
(193) Rey, R.; Hynes, J. T. *J. Chem. Phys.* **1996**, *104*, 2356.
(194) Lawrence, C. P.; Skinner, J. L. *J. Chem. Phys.* **2003**, *119*, 3840.
(195) Lawrence, C. P.; Skinner, J. L. *J. Chem. Phys.* **2003**, *119*, 1623.
(196) Rey, R.; Møller, K. B.; Hynes, J. T. *Chem. Rev.* **2004**, *104*, 1915 (in this issue).
(197) Woutersen, S.; Bakker, H. J. *Nature* **1999**, *402*, 507.
(198) Poulsen, J. A.; Nyman, G.; Nordholm, S. J. *J. Phys. Chem. A* **2003**, *107*, 8420.
(199) Pakoulev, A.; Wang, Z.; Dlott, D. D. *Chem. Phys. Lett.* **2003**, *371*, 594.
(200) Heilweil, E. J. *Science* **1999**, *283*, 1467.
(201) Kropman, M. F.; Bakker, H. J. *Science* **2001**, *291*, 2118.
(202) Kropman, M. F.; Bakker, H. J. *J. Chem. Phys.* **2001**, *115*, 8942.
(203) Kropman, M. F.; Bakker, H. J. *Chem. Phys. Lett.* **2003**, *370*, 741.
(204) Laenen, R.; Thaller, A. *Chem. Phys. Lett.* **2001**, *349*, 442.
(205) Laenen, R.; Thaller, A. *Bull. Chem. Soc. Jpn.* **2002**, *75*, 919.
(206) Laenen, R.; Thaller, A. *J. Mol. Liq.* **2003**, *103*, 291.
(207) Kropman, M. F.; Bakker, H. J. *Chem. Phys. Lett.* **2002**, *362*, 349.
(208) Kropman, M. F.; Nienhuys, H.-K.; Bakker, H. J. *Phys. Rev. Lett.* **2002**, *88*, 077601.
(209) Omta, A. W.; Kropman, N. F.; Woutersen, S.; Bakker, H. J. *Science* **2003**, *301*, 347.
(210) Nienhuys, H.-K.; Lock, A. J.; van Santen, R. A.; Bakker, H. J. *J. Chem. Phys.* **2002**, *117*, 8021.
(211) Heyne, K.; Huse, N.; Nibbering, E. T. J.; Elsaesser, T. *Chem. Phys. Lett.* **2003**, *382*, 19.
(212) Emmeluth, C.; Suhm, M. A.; Luckhaus, D. *J. Chem. Phys.* **2003**, *118*, 2242.
(213) Emmeluth, C.; Suhm, M. A. *Phys. Chem. Chem. Phys.* **2003**, *5*, 3094.
(214) Florio, G. M.; Sibert, E. L.; Zwier, T. S. *Faraday Discuss.* **2001**, *118*, 315.
(215) Petković, M.; Kühn, O. *J. Phys. Chem. A* **2003**, *107*, 8458.
(216) Graener, H.; Ye, T. Q.; Laubereau, A. *J. Chem. Phys.* **1989**, *90*, 3413.
(217) Heilweil, E. J.; Casassa, M. P.; Cavanagh, R. R.; Stephenson, J. C. *J. Chem. Phys.* **1986**, *85*, 5004.
(218) Grubbs, W. T.; Dougherty, T. P.; Heilweil E. J. *J. Am. Chem. Soc.* **1995**, *117*, 11989.
(219) Arrivo, S. M.; Heilweil, E. J. *J. Phys. Chem.* **1996**, *100*, 11975.
(220) Laenen, R.; Gale, G. M.; Lascoux, N. *J. Phys. Chem. A* **1999**, *103*, 10708.
(221) Graener, H.; Ye, T. Q.; Laubereau, A. *J. Chem. Phys.* **1989**, *91*, 1043.
(222) Laenen, R.; Rauscher, C.; Laubereau, A. *J. Phys. Chem. A* **1997**, *101*, 3201.
(223) Woutersen, S.; Emmerichs, U.; Bakker, H. J. *J. Chem. Phys.* **1997**, *107*, 1483.
(224) Laenen, R.; Simeonidis, K. *J. Phys. Chem. A* **1998**, *102*, 7207.
(225) Laenen, R.; Simeonidis, K. *Chem. Phys. Lett.* **1999**, *299*, 589.
(226) Laenen, R.; Simeonidis, K.; Ludwig, R. *J. Chem. Phys.* **1999**, *111*, 5897.
(227) Laenen, R.; Rauscher, C.; Simeonidis, K. *J. Chem. Phys.* **1999**, *110*, 5814.
(228) Laenen, R.; Rauscher, C. *Chem. Phys. Lett.* **1997**, *274*, 63.
(229) Levinger, N. E.; Davis, P. H.; Fayer, M. D. *J. Chem. Phys.* **2001**, *115*, 9352.
(230) Gaffney, K. J.; Piletic, I. R.; Fayer, M. D. *J. Phys. Chem. A* **2002**, *106*, 9428.
(231) Gaffney, K. J.; Davis, P. H.; Piletic, I. R.; Levinger, N. E.; Fayer, M. D. *J. Phys. Chem. A* **2002**, *106*, 12012.
(232) Piletic, I. R.; Gaffney, K. J.; Fayer, M. D. *J. Chem. Phys.* **2003**, *119*, 423.
(233) Asbury, J. B.; Steinel, T.; Stromberg, C.; Gaffney, K. J.; Piletic, I. R.; Goun, A.; Fayer, M. D. *Chem. Phys. Lett.* **2003**, *374*, 362.
(234) Gaffney, K. J.; Piletic, I. R.; Fayer, M. D. *J. Chem. Phys.* **2003**, *118*, 2270.
(235) Laenen, R.; Rauscher, C. *J. Chem. Phys.* **1997**, *107*, 9759.
(236) Iwaki, L. K.; Dlott, D. D. *Chem. Phys. Lett.* **2000**, *321*, 419.
(237) Iwaki, L. K.; Dlott, D. D. *J. Phys. Chem. A* **2000**, *104*, 9101.
(238) Wang, Z. H.; Pakoulev, A.; Dlott, D. D. *Science* **2002**, *296*, 2201.

CR020694P